



UIT

THE ARCTIC
UNIVERSITY
OF NORWAY

Department of Physics and Technology

Automatic Detection of Naturally Enhanced Ion-Acoustic Lines in EISCAT data

Kristian Mikalsen

Master thesis in Space Physics FYS-3931 - June 2016



Abstract

Naturally Enhanced Ion-Acoustic Lines (Neials) are small-scaled and short-lived phenomena in the ionosphere, which is widely researched internationally. At present, the search for Neials is a tedious task that has to be done through visual inspection. This is often a time-consuming process and limits the research on Neials. By automating the means of locating the Neials, the access to them will be improved and it will be more feasible to study the phenomenon.

In this thesis, routines for automatically detection Neials in EISCAT data will be presented. These routines will then be utilized to construct a program which will search for Neials. This program will be using the spectra from incoherent scatter radar experiments as the main resource. The spectra are generated using Guisdap on raw data obtained from the EISCAT database.

The program may be used such that it either picks out as many Neials as possible, as few false positives as possible, or a mixture of these two modes. In the case of picking out as many Neials as possible, the program is able to detect almost 90% of all Neials, where roughly 60% of the reported dumps are false positives. In the case of minimizing false positives, the program picks out roughly 60% of all Neials, but selects almost zero false positives.

Table of Contents

Abstract	i
Table of Contents	ii
1 Introduction.....	1
1.1 Intentions and motivation.....	1
1.2 The ionosphere.....	1
1.3 The EISCAT facility	3
2 Incoherent scatter theory	5
2.1 The incoherent scatter power spectrum.....	8
2.2 Parameters obtained from incoherent scatter	9
3 Naturally Enhanced Ion-Acoustic Lines	13
3.1 Observations.....	14
3.2 Generation mechanisms.....	17
4 Data retrieval from EISCAT	19
5 Signature of Neials in EISCAT data	21
5.1 Signature of satellites.....	22
5.2 The histogram of the spectra	24
5.3 Spectral peak	26
5.4 Power profile	29
6 Automatic detection of Neials in EISCAT data.....	35
6.1 Algorithms	35
7 Results	39
7.1 Establishing baseline	39
7.2 Algorithm performance.....	43
7.3 Discussion	47
8 Conclusion and future work	49
Code.....	51
Main program.....	51
findNeials.m.....	51
displayNeials.m.....	53
searchSpectrumHistogram.m.....	53
searchSpectrumPowerProfile.m.....	54
searchSpectrumRatio.m	55
findSpectralPeaks.m	56

Final notes	58
Acknowledgement.....	58
Bibliography.....	59
Nomenclature.....	61

1 Introduction

1.1 Intentions and motivation

In ionospheric research, many different phenomena have been discovered and are being studied. One of these phenomena is called Neial – Naturally Enhanced Ion-Acoustic Line (e.g. Rietveld et al., 1991). Neials are an enhancement in one or both of the ion-lines in the power spectra that is received by incoherent scatter radars, and will be more thoroughly discussed in section 3.

There are several incoherent scatter radar facilities around in the world, although the focus in this thesis will be on EISCAT. The data from EISCAT is publically available in a database, and currently the task of finding Neials in this database is daunting, tedious and time-consuming. There are few means of performing this task automatically today, thus limiting the research on this topic.

By improving the access to Neials, not only will current research become easier, but new and interesting correlation studies linking Neials to various physical phenomena may open up (e.g. substorms, particle precipitation, variations in the Earth's magnetic field). In this thesis, various methods for automatic detection of Neials will be discussed. These methods will then be used in the development of a program that can be applied to large datasets to automatically find Neials quickly and easily.

1.2 The ionosphere

The ionosphere is the ionized section of the Earth's upper atmosphere. The ionosphere may be divided up into a few layers, the D-, E- and F-layers. The distinctions between the layers are not always clear, however, except for under certain conditions. At present, it is more common to speak about regions rather than layers.

The D-region, which is located between 60 *km* and 90 *km* altitude, is governed by complicated chemical reactions. In this region, the most abundant neutral species are N_2 , O_2 and O . Both positive and negative ions may be found in this region. The most abundant ions are molecular, such as NO^+ and O_2^+ , as illustrated in Figure 1.

The E-region is located between 90 *km* and 150 *km* altitude. Historically, this name was given due to the reflections of electric fields. In this region, NO^+ and O_2^+ are still dominant ions; chemical reactions are still very important in this region, although not as complicated as in the D-region. It is also within this region that the aurora occurs, where the height distribution of the auroral arcs peaks at roughly 100 *km* altitude (Brekke, 2013).

The F-region extends from 150 *km* to more than 500 *km* altitude. It is often divided into two regions, the F1- and F2-regions. In the lower parts of the F-region atomic oxygen, O^+ , is dominant. At higher altitudes atomic hydrogen, H^+ , is becoming more abundant, though not as common as O^+ . The electron number density peaks in the F2-region, where the number density is on the order of $10^{11} m^{-3}$, whereas the neutral number density is on the order of $10^{15} m^{-3}$. The plasma is thus only partially ionized, meaning that collisions between charged and neutral particles must be considered. It is in the F-region that the majority of Neials are occurring (Ogawa et al., 2011).

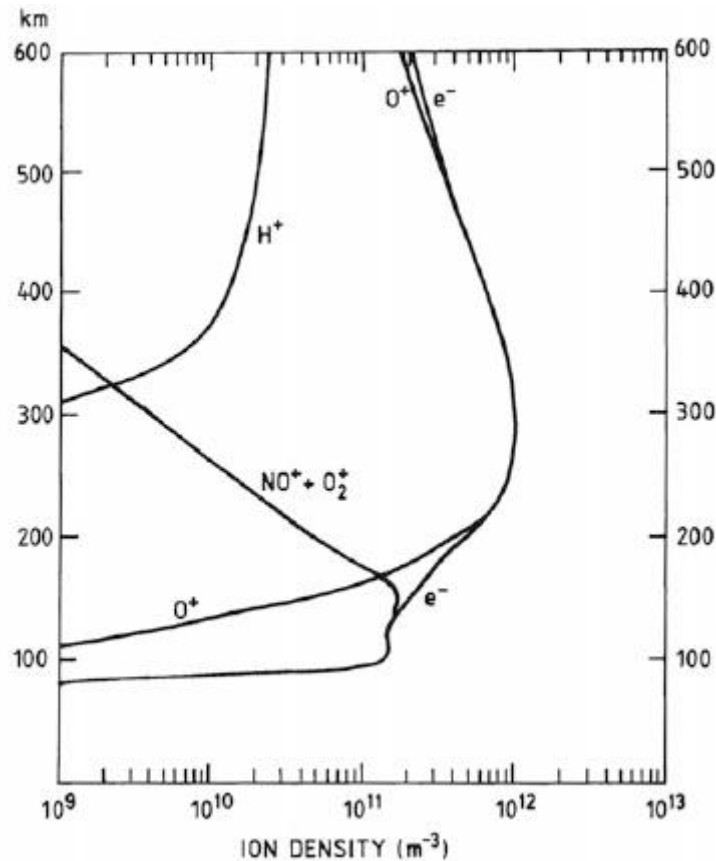


Figure 1: Number density profile for the most typical ions in the ionosphere between 100 km and 600 km, including the corresponding electron number density profile (from Brekke, 2013).

The temperature of the ionosphere is governed by the amount of solar UV radiation that is absorbed in the thermosphere. This radiation is able to ionize molecules and atoms, forming free electrons. These electrons carry some of the excess energy obtained from this ionization process with them. Due to the larger heat capacity of the electrons, they tend to be hotter than the ions, which transfer much of their excess energy to the neutral gas. The ion temperature is therefore lower than that of electrons, although greater than that of the neutral gas.

The ionosphere may be viewed as a shell of plasma that surrounds the Earth. The number density of electrons varies with altitude and a typical profile is displayed in Figure 2. Below the D-region there are virtually no free electrons. The electron number density depends on the time of day and the activity of the Sun. The more active the Sun is, the more ionization takes place in the atmosphere.

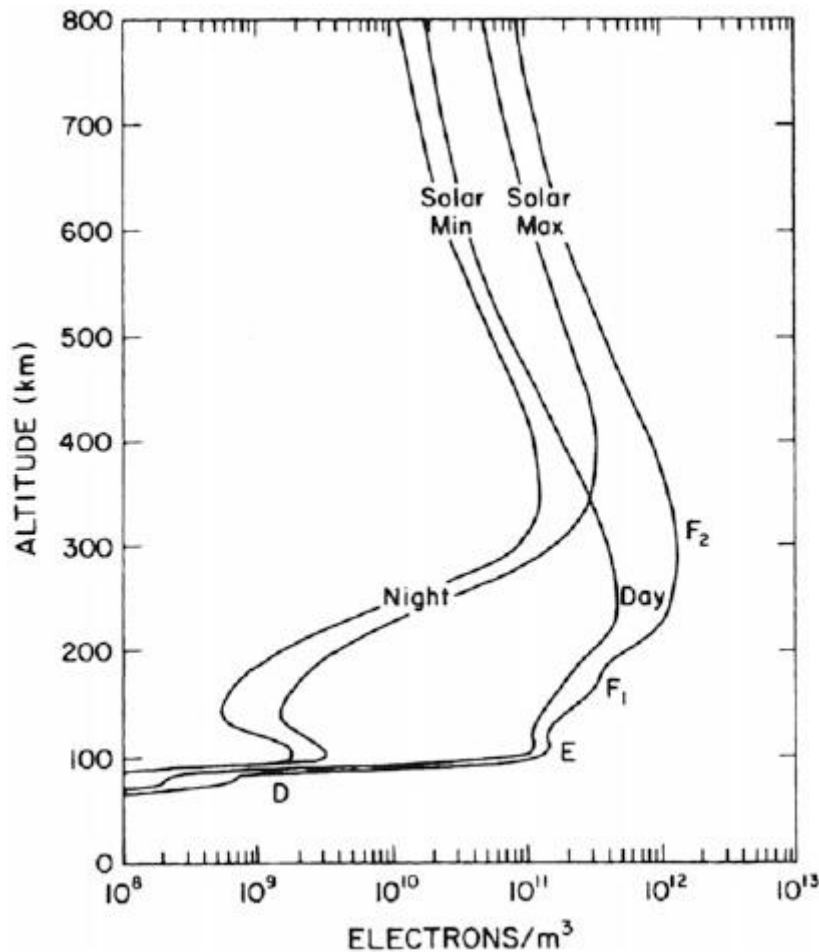


Figure 2: The typical electron number profile shown for sunspot maximum and minimum during day- and nighttime (from Brekke, 2013).

1.3 The EISCAT facility

The EISCAT (European Incoherent Scatter Scientific Association)¹ conducts research in the polar atmosphere. EISCAT operates three different radar systems, two of which are located in Ramfjordmoen, near Tromsø, Norway, and one is located in Svalbard. There are additional receiver stations located in Sodankylä, Finland and Kiruna, Sweden.

The antennas located in Ramfjordmoen near Tromsø, the UHF (ultra-high frequency) and VHF (very high frequency) radars, operate at roughly 928 MHz and 224 MHz, respectively. The UHF radar has a peak transmitter power of more than 2 MW, and consists of a 32m steerable parabolic antenna. The VHF radar operates at a peak power of 1.6 MW, using a 4x 30m-by-40m parabolic cylinder antenna. The radar may be steered in the meridional plane from an angle between vertical to 60° north of the zenith.

The EISCAT system has one receiver in Ramfjordmoen, with two more receivers located in Sodankylä, Finland and Kiruna, Sweden. Due to this trio of receivers, tri-static measurements are possible.

¹ EISCAT Scientific Association, <https://www.eiscat.se>

The EISCAT Svalbard Radar (ESR) is located near Longyearbyen, Svalbard. The facility consists of two antennas, one which is 42m in diameter and is fixed along the geomagnetic field, and one which is 32m in diameter and is fully steerable.

The locations of the EISCAT facilities may be summarized as

Location	Tromsø	Kiruna	Sodankylä	Longyearbyen
Geographic latitude	69°35' N (69.58°)	67°52' N (67.87°)	67°22' N (67.37°)	78°09' N (78.15°)
Geographic longitude	19°14' E (19.23°)	20°26' E (20.43°)	26°38' E (26.63°)	16°01' E (16.02°)
Altitude	86 m	418 m	197 m	445 m

Table 1: Geographical location of the EISCAT facilities (EISCAT Scientific Association, 2016).

The technical specifications of the systems may be summarized as

Location	Tromsø		Longyearbyen
Band	VHF	UHF	UHF
Transmitter frequencies	222.8 - 225.4 MHz	926.6 - 930.5 MHz	498.0 - 502.0 MHz
Transmitter	1 klystron	2 klystrons	16 klystrons
Peak power	1.6 MW	2 MW	1 MW
Average power	200 kW	250 kW	250 kW
Pulse duration	1 μ s - 2.0 ms	1 μ s - 2.0 ms	0.5 μ s - 2.0 ms
Minimum interpulse	1.0 ms	1.0 ms	0.1 ms
Receiver frequencies	214.3-234.7 MHz	921.0-933.5 MHz	485.0-515.0 MHz
Receiver	Analog	Analog	Analog
System temperature	250-350 K	90-110 K	65-80 K
Baseband channels	6	6	2 \times 6
Antenna	Four 30 \times 40 m steerable parabolic cylinders	32 m steerable parabolic dish	42 m fixed and 32 m steerable parabolic dishes
Gain	46 dBi	48.1 dBi	44.8 dBi or 42.5 dBi
Polarisation	Circular	Circular	Circular

Table 2: Some of the technical specifications of the EISCAT facilities (EISCAT Scientific Association, 2016).

2 Incoherent scatter theory

The term *incoherent scatter* refers to the very faint scatter from ionized gas, specifically from electrons. When an electromagnetic wave propagates through a medium that has spatial variations in the refractive index or dielectric constant, it cannot propagate unperturbed. The energy of the wave will be scattered in all directions due to the refractive index variations. This scattering is caused by fluctuations in the plasma density. Electrons are charged and discrete particles, not a continuous medium.

An incoherent scatter radar experiment is carried out by transmitting a high-power electromagnetic wave into the ionosphere, illustrated in Figure 3a. Electrons that are hit by this beam will be accelerated, and as such they will also emit electromagnetic radiation. This can be received by the radar, albeit faint, as scattered radiation. The ions' contribution to this signal can be neglected, due to their much larger inertia than the electrons – the ions can be said to be too heavy to respond to the incoming radiation, thus the scatter is mostly a product of the electrons.

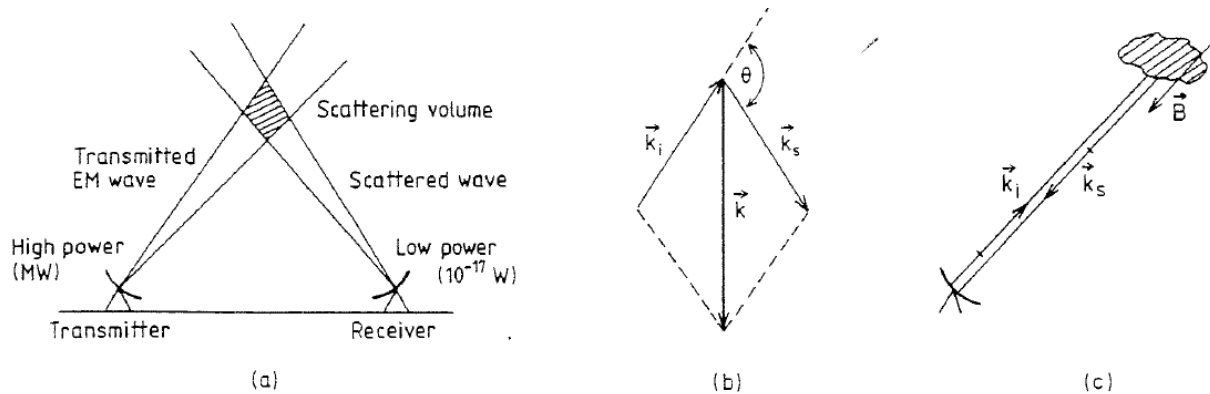


Figure 3: (a) The setup of the incoherent scatter radar experiment. (b) The relation between the incident wave, \vec{k}_i , the scattered wave vector \vec{k}_s and the wave vector $\vec{k} = \vec{k}_s - \vec{k}_i$. (c) A special case where $\vec{k}_s = -\vec{k}_i$, or equivalently, $\theta = \pi$. (From Bjørnå, 2005)

The scattered signal will have the same frequency as the incoming electromagnetic radiation (the radar frequency), although it will have a bandwidth, spanning multiple nearby frequencies. This is due to the Doppler broadening, which is caused by the random thermal motion of electrons. In addition, due to the bulk movement of the plasma, the collective motion of the particle species, there will be a Doppler shift of the frequency.

To be able to understand the spectrum that is the result of an incoherent scatter radar experiment, a rigorous mathematical model is needed. While such an analysis is beyond the scope of this thesis, a simpler description will be provided. The reader is referred to Trulsen and Bjørnå (1975) for a more satisfying argumentation. Before going into greater details, however, it is relevant to introduce some useful quantities.

For charged particles, the *Debye length* is a measure of the sphere of influence around a test particle that is present in a plasma. The Debye length is defined, for electrons and ions respectively, as

$$\lambda_{De} = \sqrt{\frac{\epsilon_0 T_e}{n_0 e^2}}, \quad \lambda_{Di} = \sqrt{\frac{\epsilon_0 T_i}{n_0 e^2}} \quad (2-1)$$

Here ϵ_0 is the permittivity of free space, $T_{e,i}$ are the electron and ion temperatures, respectively. n_0 is the mean number density and e is the electron charge. The total Debye length is written as

$$\frac{1}{\lambda_D^2} = \frac{1}{\lambda_{De}^2} + \frac{1}{\lambda_{Di}^2} \quad (2-2)$$

Any particles that are much further away from the test particle than this distance, $r \gg \lambda_D$, will not be affected by the test particle – it has been *shielded out* by the plasma. In the ionosphere, the Debye length is typically on the order of a few millimeters to a few centimeters.

There are two main approaches for the development of a mathematical theory, the microscopic and the macroscopic approach. The microscopic approach is commonly referred to as the “dressed particle” approach, where each individual particle in the plasma, including their neutralizing (Debye shielding) moving cloud is considered. The macroscopic approach considers the fluctuations in the plasma to be made out of a sum of acoustic-like waves.

The results from both approaches are consistent with each other, although the insight they may give in the physical processes in scattering is different. In this thesis, the macroscopic approach will be utilized, as the transition from it to the incoherent scatter spectra (See section 2.1) is better suited in order to explain the Neials.

Plasma waves

If the plasma is perturbed slightly from the equilibrium state, electric fields will build up, resulting in particles being dragged towards their equilibrium positions. Due to their inertia, the particles will overshoot their positions and start to oscillate with a given frequency. This frequency is given by ω_{pe} , which is known as the *electron plasma frequency*. It is defined as

$$\omega_{pe} = \sqrt{\frac{n_e e^2}{m_e \epsilon_0}} \quad (2-3)$$

where n_e is the number density of the electrons and m_e is the mass of the electron.

These oscillations are a high frequency oscillation (the electron plasma frequency is on the order of MHz), meaning that ions are unable to keep up with them and can in principle be seen as stationary. These oscillations do not propagate through the plasma, however. By introducing the thermal motion, $v_{th,e} = \sqrt{\kappa T_e / m_e}$, where κ is the Boltzmann constant, the result will be *electron plasma waves*, also known as *Langmuir waves*, which do propagate through the plasma. The dispersion relation for these waves may be written as

$$\omega = \sqrt{\omega_{pe}^2 + 3k^2 v_{th,e}^2} = \omega_{pe} \sqrt{1 + 3k^2 \lambda_{De}^2} \quad (2-4)$$

where $\omega_{pe}^2 \lambda_{De}^2 = v_{th,e}^2$. The group velocity $d\omega/dk = 3kv_{th,e}^2/\omega$ now depends on k (where $k = |\vec{k}|$ is the wave vector magnitude), thus the wave is dispersive.

Ion-acoustic waves are waves that propagate at lower frequencies (on the order of kHz), slow enough for the ions to respond. It can be shown that by treating the ions as mobile, this will result in

$$\omega = kC_s \quad (2-5)$$

where $C_s = \sqrt{(\gamma_e \kappa T_e + \gamma_i \kappa T_i)/m_i}$ is the *ion-acoustic*, or *ion-sound*, speed, if described by a fluid model. Here, $\gamma_{e,i}$ denotes the specific heats C_p/C_V for electrons and ion, respectively. This model, however, cannot describe Landau damping, which is important to the understanding of the spectrum. In kinetic theory, a central element is the particle *distribution function*. In general it is a function of position, velocity and time, $f = f(\vec{x}, \vec{v}, t)$. In the case of a uniform, isotropic and stationary plasma, f is a function of velocity only, $f = f(\vec{v})$. One distribution function that is particularly important, is the Maxwellian distribution, which in the one-dimensional case may be written as

$$f_M(v_x) = \sqrt{\frac{m}{2\pi\kappa T}} \exp\left(-\frac{(v_x - v_d)^2}{2v_{th}^2}\right) \quad (2-6)$$

v_x is the particle speed in the x-direction, v_d is the drift velocity in the same direction and m is the mass of the particle. Figure 4 shows a typical ion-Maxwellian distribution. In the case of $T_e/T_i = 3$, the phase velocity lies well within the ion velocity distribution. Due to there being more slow ions than fast ones near the wave phase velocity, the wave is damped. In the case of $T_e/T_i = 15$, the slope of the distribution is very small at the wave phase velocity. There are few ions near the wave phase velocity and there are almost as many fast ions as slow ions, thus the damping is small.

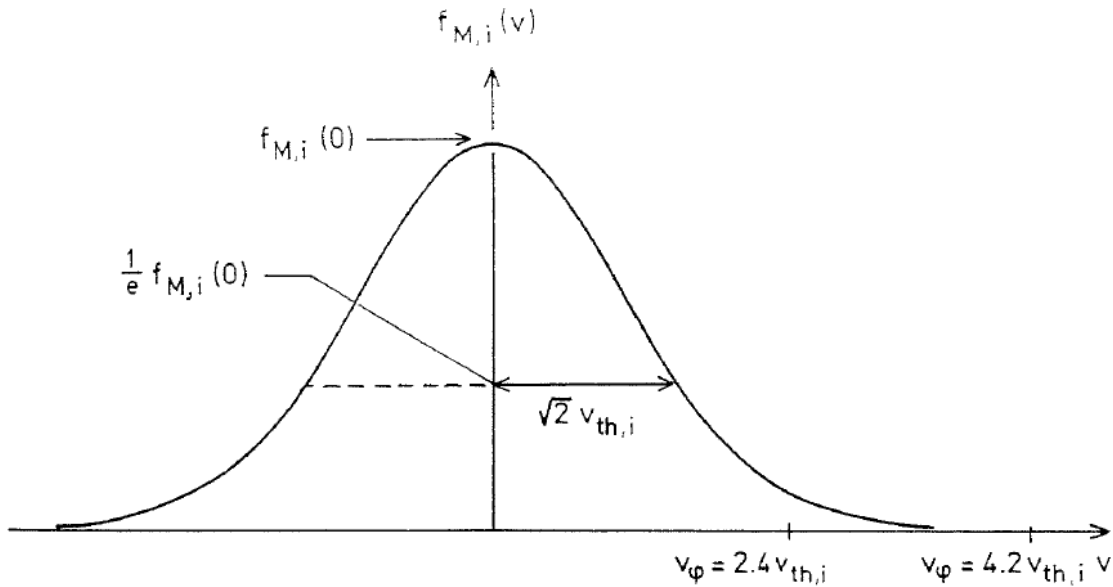


Figure 4: Illustration of a Maxwellian ion velocity distribution $f_{M,i}(v)$. The ion thermal velocity is $v_{th,i} = \sqrt{\kappa T_i/m_i}$. The phase velocities of the ion-acoustic waves are given as $v_{\phi} = 2.4 v_{th,i}$ and $v_{\phi} = 4.2 v_{th,i}$ for $T_e/T_i = 3$ and $T_e/T_i = 15$, respectively (from Bjørnå, 2005).

In kinetic theory the wave frequency is a complex value, $\omega = \omega_r + i\omega_i$, where the subscripts r and i denote the real and complex parts, respectively. The first term represents an oscillation in time at frequency ω_r and the last term represents a damping if $\omega_i < 0$ and a growth if $\omega_i > 0$. This damping is called *Landau damping*.

For Langmuir waves, kinetic theory yields

$$\omega_r = \omega_{pe} \sqrt{1 + 3k^2 \lambda_e^2}, \quad \omega_i = -C \frac{\omega_{pe}}{(k \lambda_e)^3} \exp\left(-\frac{1}{2k^2 \lambda_e^2}\right) \quad (2-7)$$

where $C = \sqrt{\pi/8} \cdot e^{-3/2}$.

Assuming a weak damping, $|\omega_i| \ll \omega_r$ (equivalent to $T_e \gg T_i$), kinetic theory yields the result

$$\omega_r = \frac{k C_s}{1 + k^2 \lambda_e^2} \quad \omega_i = -\sqrt{\frac{\pi}{8}} \frac{\omega_r}{(1 + k^2 \lambda_e^2)^{3/2}} \left[\left(\frac{T_e}{T_i}\right)^{3/2} \exp\left(-\frac{T_e/T_i}{2(1 + k^2 \lambda_e^2)} + \sqrt{\frac{m_e}{m_i}}\right) \right] \quad (2-8)$$

for ion-acoustic waves. The damping is determined by the ratio T_e/T_i , where the larger this ratio is, the less the damping will be.

Both the Langmuir waves and the Ion-acoustic waves will contribute to the incoherent scatter spectrum. Due to Landau damping and thermal motion, the spectral bandwidth of the contributions will be wider, although centered on the electron plasma and ion-acoustic frequencies, respectively. The end result is a double-humped spectrum with a pair of plasma lines shifted by approximately ω_{pe} away from the center.

Waves represent an ordered motion of the particles, which is why they are of such great importance to the incoherent scatter spectrum. Waves enhance the scattering effects at the wave frequency.

2.1 The incoherent scatter power spectrum

The mathematical expression for the power spectrum as described by Bjørnå (2005) is written as

$$S(\vec{k}, \omega) = C \frac{n_e}{k} \left[f_e\left(\frac{\omega}{k}\right) \left| 1 + \frac{Z_e(\vec{k}, \omega)}{\epsilon(\vec{k}, \omega)} \right|^2 + f_i\left(\frac{\omega}{k}\right) \left| \frac{Z_i(\vec{k}, \omega)}{\epsilon(\vec{k}, \omega)} \right|^2 \right] \quad (2-9)$$

Here, C is a numerical constant, f_e and f_i are the electron and ion velocity distribution functions in the direction along the magnetic field. ϵ is the complex dispersion function, which is given as $\epsilon = \epsilon_r + i\epsilon_i$, and has the form $\epsilon(\vec{k}, \omega) = 0$. Here, $\epsilon = 1 - Z_e - Z_i$, and Z_e and Z_i represents the integrals involving the electron and ion velocity distributions, respectively.

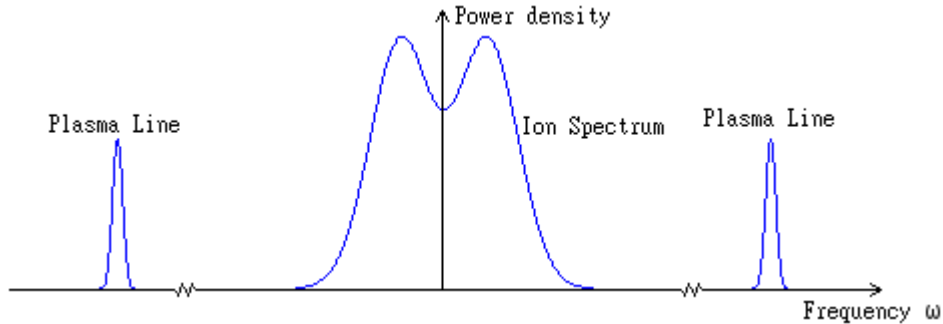


Figure 5: A typical power spectrum from the ionospheric F-region. The spectrum is centered on the transmitter frequency, where the ion lines are shifted by kilohertz and the plasma lines are shifted by megahertz. The figure is not to scale.

A typical shape of a power spectrum is illustrated in Figure 5. The center part of the spectrum is known as the *ion spectrum* or *ion line* (Bjørnå, 2005), and the pair of lines that are shifted away from the center are known as the *plasma lines* (Bjørnå, 2005).

The shape of this spectrum reveals the existence of waves in the ionospheric plasma. The properties of the Langmuir waves and the ion-acoustic waves along the geomagnetic field can explain the shape of the backscatter spectrum. The equations (2-8) and (2-9) are derived for the case of no magnetic field, which means they may be directly used to describe waves along the magnetic field.

Langmuir waves are high-frequency waves at the frequency ω_r given by equation (2-7). If $k^2\lambda_e^2$ is small, the Landau damping will be small and ω_r will satisfy $\epsilon(\vec{k}, \omega_r) = 0$. Examining equation (2-9) in this situation reveals that the last term vanishes. Here, ω/k lies far out in the tail of the ion velocity distribution function f_i , such that $f_i(\omega/k) \approx 0$. In the dispersion function, only electrons contribute and the first term in equation (2-9) is only depending on electrons. Ions do not contribute here, which is consistent with the theory; ions are too slow to respond in time. At the frequencies $\omega = \pm\omega_r$, the real part of ϵ is zero and the imaginary part will be small if $k^2\lambda_e^2$ is small. These frequencies represent the plasma lines in Figure 5. The upshifted line ($+\omega_r$) and downshifted line ($-\omega_r$) represents a Langmuir wave traveling towards and away from the radar, respectively. The damping of the Langmuir wave determines the width of the plasma lines (Chen, 1984).

In the case where $T_e \gg T_i$, the ion-acoustic waves will be weakly damped. This leads to a small ϵ_i and ϵ_r is zero at the frequencies $\omega = \pm kC_s$. This gives rise to two spectral lines at the frequencies $\pm kC_s$. Similarly as for the Langmuir waves, the upshifted wave travels towards the radar, the downshifted wave travels away from the radar. The condition $T_e \gg T_i$ is not typically strictly satisfied in the ionosphere, however. Commonly ion-acoustic waves are more strongly damped which results in the spectral lines being broadened and merge into one double-humped line as seen in Figure 5.

The main bulk of the description so far has focused on the situation $k^2\lambda_e^2 \ll 1$. In this situation, the wavelength of the radar is much larger than the Debye length. The particles are able to effectively shield out the influence of the wave, thus they operate in a collective behavior and are correlated. In the opposite case, where $k^2\lambda_e^2 \gg 1$, the radar wavelength would be much smaller than the Debye length. This is not typically the case in the ionosphere, however, where the Debye length is usually on the order of mm or cm. For wavelengths much shorter than the Debye length, the particles would be unable to shield themselves. As such, the power spectrum would be a spectrum from a distribution of independent and uncorrelated electrons. The shape would be the same as the electron distribution function, only mapped from velocity space to frequency space.

2.2 Parameters obtained from incoherent scatter

There are several parameters that can be measured directly from the incoherent scatter, as well as a variety of parameters that may be derived. For a thorough review of the various parameters, the reader is referred to Beynon and Williams (1978). A brief description of some of the parameters will be provided in this thesis.

Electron density

The electron density as a function of altitude may be measured in several ways.

The total power returned during an incoherent scatter depends on the number of scatterers, which are the electrons. The total power, that is the area under the incoherent scatter spectra, is therefore a measure of the density of electrons.

It is also possible to obtain the density of electrons from Faraday rotation. In this case, knowledge of the magnetic flux density is required, as well as the angle between the magnetic field lines and the path of the signal.

For wavelengths much larger than the Debye length, it is also possible to extract information about the electron density from the plasma lines in the power spectrum. At night, the plasma lines are too weak to be detected, although at daytime they may be significantly enhanced, up to a factor of 50. The plasma lines are shifted from the transmitter frequency by approximately $\pm f_p = \pm 9n_e^{1/2}$, where n_e is the electron number density.

Electron and ion temperature ratio

When the ratio $T_e/T_i \gg 1$, the ion-acoustic waves are weakly damped. This in turn means that the ion-lines in the incoherent scatter spectra will be narrower, becoming two peaks approximately centered on the frequencies $\pm kC_s$. In the case where $T_e \approx T_i$, however, the ion-acoustic waves are strongly damped. Here, the ion-lines will be broader and tend towards a single-humped spectrum.

The peak-to-valley ratio and the sharpness of the spectral peaks is thus a measure of the ratio of the electron and ion temperature. More information about the temperature may also be extracted from the incoherent scatter spectra. The separation between the two ion-lines depends upon the temperature ratio T_e/T_i , but also the ratio between the ion temperature and mass, T_i/m_i . The greater the ion temperature is, the further apart the ion-lines will be, widening the spectra.

The two top panels in Figure 6 illustrate the effects the variations in electron and ion temperature has on the incoherent scatter spectra.

Plasma bulk velocity

When a plasma has a bulk movement, the entire spectrum as a whole will be Doppler shifted. By measuring this Doppler shift, it is possible to determine the velocity of the plasma movement in the direction of \vec{k} . It is only possible to measure one component of the bulk velocity, as the velocity component perpendicular to \vec{k} has a zero Doppler shift. Suppose, however, that three different stations that are positioned suitably relative to each other, and they all take a measurement simultaneously. In this case, the bulk velocity of the plasma, the three components of the drift velocity, may be fully determined.

A great precision is needed when making these measurements, however. The Doppler shift varies from the base frequency by a very small amount, on the order of 10^{-1} kHz. As such, an accurate measurement of the whole spectrum is required in order to determine the bulk velocity.

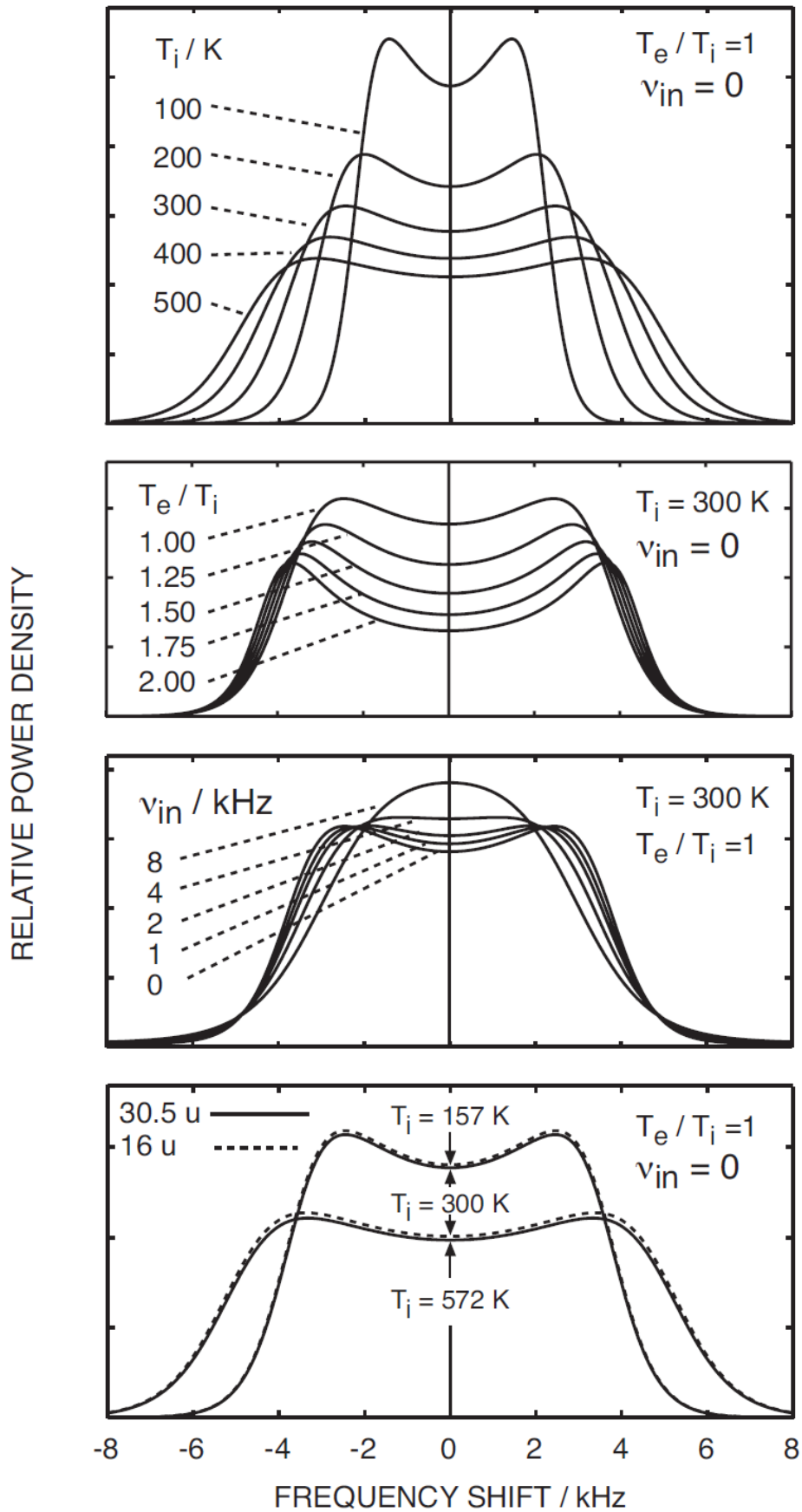


Figure 6: The incoherent scatter spectra dependency on various ionospheric parameters (from Nygrén, 1996).

Other parameters

It is possible to measure more parameters from the incoherent scatter spectra. Parameters such as the ion-neutral collision frequency, the spectrum of suprathermal electrons, and the electrical current density may be obtained, although only from a limited range of altitudes or under favorable conditions.

From all the parameters that may be measured directly, several parameters may be estimated. These parameters include the electric field, ionospheric conductivities (Hall and Pederson conductivities), the neutral wind velocity, the neutral temperature and the downward flux of heat from the exosphere.

The reader is referred to Beynon and Williams (1978) for a complete discussion of the various parameters that may be measured and derived from the incoherent scatter spectra.

3 Naturally Enhanced Ion-Acoustic Lines

Neials, or Naturally Enhanced Ion-Acoustic Lines, as it is an acronym for, is an enhancement in one or both of the ion lines. The regular conditions are illustrated in Figure 7, in the rightmost panel, whereas the enhancements are presented in the two leftmost panels. These enhancements may span multiple gates in the dump. It is clear that in the leftmost panel, there is an enhancement in the downshifted ion line at altitudes spanning from about 500 km to 600 km, and in the middle panel an enhancement can be seen in the upshifted line, in altitudes spanning from about 630 km to 700 km.

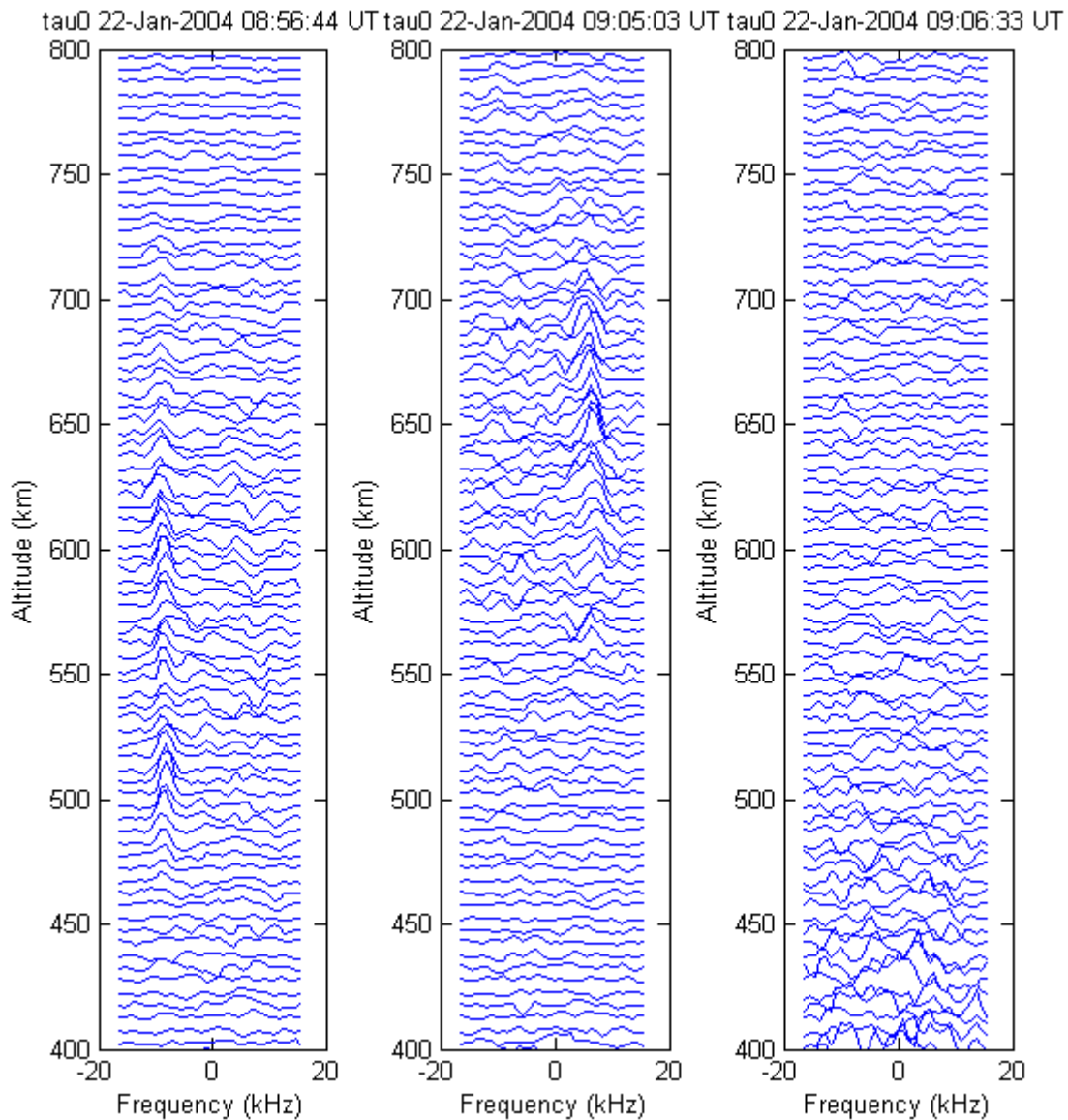


Figure 7: The spectra contained in two dumps obtained from the ESR 42m antenna. The magnitudes of the spectra have been normalized. The rightmost panel does not contain Neials.

The enhancements in ion-acoustic lines were first predicted as early as 1962 by Rosenbluth and Rostoker (1962). For close to thirty years, the enhancements were observed by various radar facilities, although they were dismissed as an effect of satellites and other hard objects crossing the

radar beam. It took until 1988 that Foster et al. (1988), using the Millstone Hill radar², were able to demonstrate that some of these enhancements had a physical origin.

Not many years later, other radar facilities reported similar observations. The EISCAT radars in Tromsø, which is located in the auroral zone, were used by Collis et al. (1991) and Rietveld et al. (1991) to observe this phenomenon. Buchert et al. (1999) observed for the first time Neials on Svalbard, using the EISCAT Svalbard Radar.

In the time following the observations, several papers have been published in order to explain how these events occur and the physical mechanisms behind them (e.g. Foster et al., 1988; Collis et al., 1991; Rietveld et al., 1991; Wahlund et al., 1992b; Forme, 1993 and 1999). These processes are yet to be properly understood, however. A common theme for all current explanations is an instability process where particle precipitation plays an important role.

Neials have been observed together with many different geophysical phenomena where particle precipitation, either directly or indirectly is involved, which is why particle precipitation is believed to be a key factor to Neials' generation mechanisms. These observations include intense ion outflows (Wahlund et al., 1992a; Forme and Fontaine, 1999), enhanced plasma lines (Strømme et al., 2005), severe geomagnetic disturbances, density enhancements in the E-region, electric heating in the F-region (Rietveld et al., 1991).

3.1 Observations

The enhancement of the ion-acoustic lines may happen in one or both of the lines. The line that is in the negative part of the spectrum (typically the left side) is the downshifted line, and the line in the positive part is the upshifted line. The terms *down-* and *upshifted* refer to the fact that the frequency of the signal is lower and higher, respectively, than the base frequency (the transmitted frequency).

At lower altitudes, the right ion-line is typically enhanced more than the left, and at higher altitudes, the left ion-line is typically enhanced more than the right (Lunde et al., 2007; Grydeland et al., 2003). The case where both ion-lines are enhanced simultaneously is a less common event. Lunde et al. (2007) reports finding 41 Neials, where 9 had an enhancement in both ion-lines simultaneously.

Neials are very burst-like in nature, where they may be seen in one 6.4-s dump, but not in the next or the previous one. The timescales on which these enhancements take place are very brief. It has been shown that the enhancements last for a time on the order of seconds or less (Grydeland et al., 2003).

A couple of dates that have been examined are July 6th, 2000, from 04:30:00 UT to 12:00:00 UT and 22nd January, 2004, from 08:45:00 UT to 10:00:00 UT. Raw 6.4-s dumps from the ESR 42m antenna have been examined by visual inspection, revealing a good number of various Neials. More than 70 dumps with Neials of varying enhancements have been observed between these two timeframes combined.

² MIT Haystack Observatory, <http://www.haystack.mit.edu>

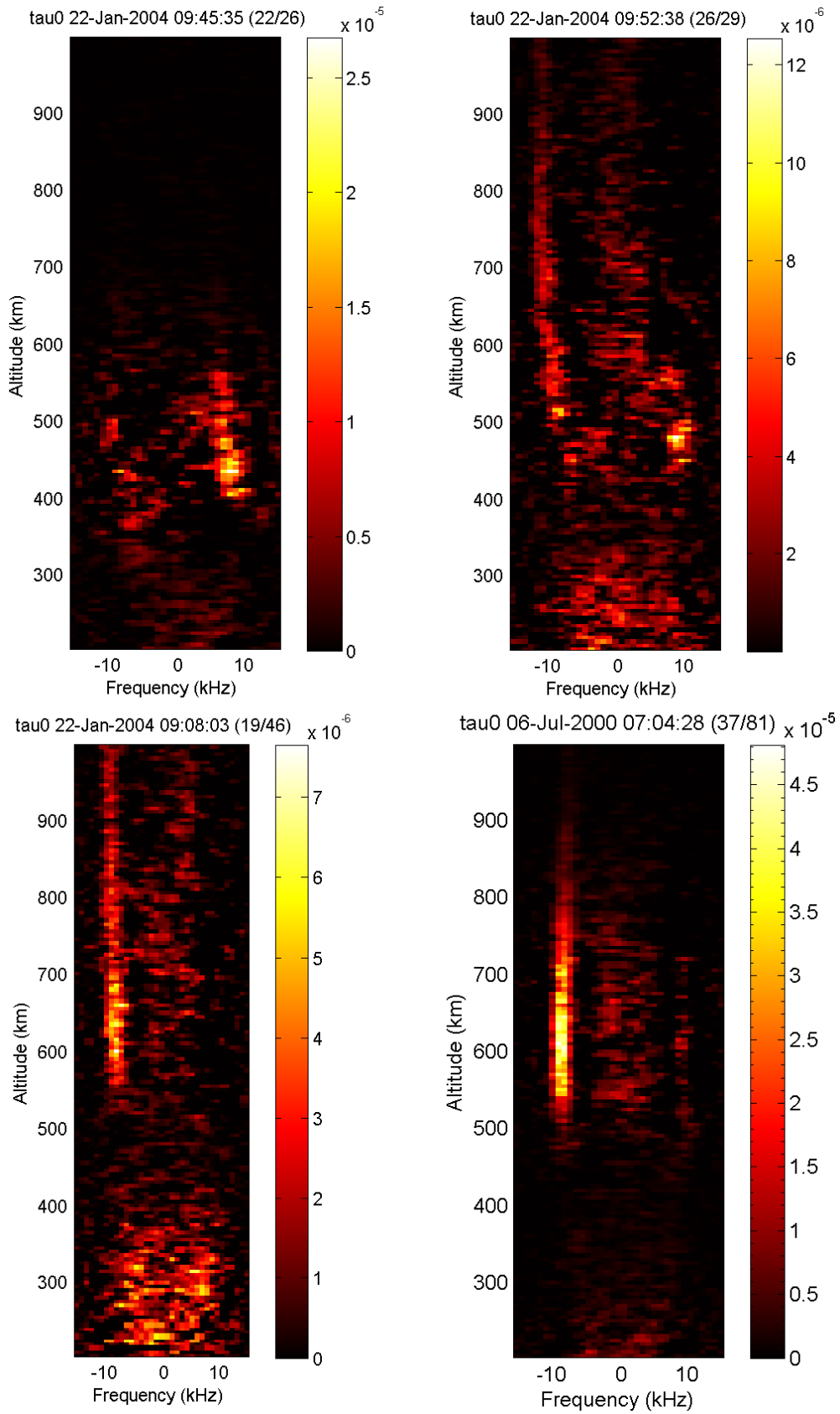


Figure 8: Some Neials that were found using the ESR 42m antenna. Top left: a short Neial, with a blob-like structure to it. Top right: A long Neial, which is slightly bent near an altitude of 600 km. There is a blob-like structure on the upshifted line just below 500 km. Bottom left and right: typical Neials that are long and clear.

In these dumps, Neials are typically found shifted between 5-10 *kHz* away from the transmitter frequency. The bandwidth of the enhanced line is typically between 2 *kHz* and 5 *kHz*, although the width and position of the line in frequency space may vary with altitude. In the incoherent scatter spectra, Neials often appears at a fixed frequency, spanning a range of altitudes. In certain cases there is a shift in the frequency (Figure 8, top-right panel) and the Neial appears to be bent in frequency space.

Other shapes that are seen in the incoherent scatter spectra are small, almost blob-like structures (Figure 8, top-left panel). Typically the enhancements can be seen in many consecutive gates, corresponding to a distance on the order of 100 *km*, similar to the Neials that are shown in Figure 8, bottom-half panels.

In these observations, a typical altitude range where the Neials are observed is between 300 and 900 *km* altitude, although some Neials extends beyond 1000 *km* altitude. In general, even though Neials are rarely seen below 200 *km* or above 1000 *km*, they have been observed as far down as about 146 *km* (Rietveld et al., 1991) and as high as 1600 *km* (Ogawa et al., 2006).

Characteristics

Neials display an enhancement in one or both of the ion lines, as previously mentioned. These enhancements have been presented in Figure 7 and Figure 8 in two different ways, where the former figure displays the spectra in each dump individually and the latter displays the spectra as intensity plots.

While the enhancements may be seen in one or both the ion lines, these enhancements also affecting the power profile as function of altitude. This is illustrated in Figure 9, where there is a significant boost in the signal in the altitudes ranging from about 400 *km* to 600 *km*. It should be noted that the Neials are prominent due to the ordered motion of the particles; this does not mean that the incoherent scatter spectra reflect true physical values when a Neial is present, as the standard analysis breaks down under these conditions.

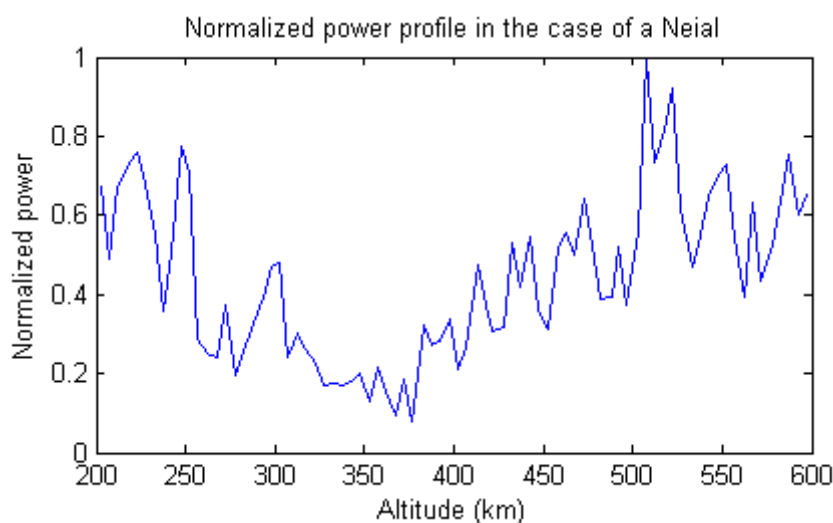


Figure 9: The contribution from a Neial is typically significant in the power profile. There is a clear contribution in the altitudes spanning from 400 *km* to 600 *km*.

3.2 Generation mechanisms

There has been proposed multiple theories to explain the Neial phenomenon, although it is yet to be fully understood. In literature there are three main theories to explain how Neials are generated. These theories are current-driven instabilities (also known as ion-electron two-streak instability), ion-ion two-stream instability and parametric decay of Langmuir waves.

Current-driven instabilities

Rietveld et al. (1991) suggests that the strong asymmetrical enhancements that can be observed in the ion-lines are due to a strong differential flow between thermal ions and thermal electrons. With this explanation, the asymmetry is explained as there being more electrons scattering radio waves on one side of the ion velocity distribution than the other. In order to detect such asymmetry, the electrons would have to be drifting at a velocity that is a detectable fraction of their thermal velocity.

The ion-acoustic instabilities are then driven by thermal electrons, which would require a large field-aligned current on the order of 1 mA/m^2 . Currents such as this have been detected by the Ørsted Satellite (Neubert and Christiansen, 2003). The ion-line that is enhanced is said to be determined by which direction the electrons are moving, assuming the ions are stationary. If the electrons move towards the radar, the enhancement can be found in the upshifted line.

An issue with the current-driven explanation, however, is that it does not account for simultaneously up- and downshifted ion lines. Rietveld et al. (1991) addresses this issue by stating that the simultaneous enhancements may be a temporal feature, where electrons are moving in one direction at first, then changing direction. Grydeland et al., (2003) has shown that the timescales of the enhancements are very brief, on the order of 10^{-1} s , where simultaneous enhancement has taken place. This suggests that the explanation of the simultaneous enhancement proposed by Rietveld et al. (1991) is not sufficient. Another explanation that was proposed by Rietveld et al. (1991) was that what can be observed are very narrow structures. It is presently believed that such structures are unlikely to occur in the width of the beam, which is on the order of km in the ionosphere.

Ion-ion two-stream instability

Wahlund et al. (1992b) focused on the strong field-aligned bulk ion outflows that were observed by the EISCAT incoherent scatter radar in the auroral topside ionosphere and at mid-latitudes using the Millstone Hill radar³. Such ion outflows were observed associated with auroral arcs, topside electron temperature enhancements (up to 8000 K) and soft particle precipitation with energy levels on the order of 100 eV (Wahlund et al., 1992a), conditions which are favorable for the ion-ion two-stream instability.

The ion-ion instability is driven by a large relative drift between two different ion populations. As an example, this could be between O^+ and a beam of H^+ . This instability is able to develop as long as the ion drift velocities are on the order of the ion thermal velocities and $T_e/T_i \geq 3$. For drifts that are twice that of the ion thermal speed, it is possible to obtain enhancements of one or two orders of magnitude in one or both the ion lines.

³ MIT Haystack Observatory, <http://www.haystack.mit.edu>

In order to achieve the relative drifts that are required, a sufficient acceleration of H^+ is required, which may be possible in the upper altitudes. At the lower altitudes, NO^+-O^+ is proposed to be a possible candidate for the instability process, although the higher collision frequency is an obstacle. The charged particles will collide more often with the neutral atmosphere in this region. If a process is able to accelerate O^+ or NO^+ , however, instability processes could occur.

The ion-ion two-stream instability has a couple advantages over the current-driven instability. The ion-ion two-stream instability does not require a large current, which the theory proposed by Rietveld et al. (1991) does. Additionally, the theory proposed by Wahlund et al. (1992b) is capable of explaining the simultaneous enhancements of both the ion-lines.

Parametric decay of Langmuir waves

Both the current-driven instability and the ion-ion two-stream instability have issues explaining certain characteristics that can be observed in relation to Neials. An additional theory has been proposed by Forme (1993 and 1999). It is suggested that the enhancement in the ion-acoustic lines are due to the decaying of Langmuir waves according to the process $l \rightarrow l' + s$.

Here, l is a “pump” Langmuir wave that is produced by a soft electron beam with energy levels of 10 to 500 eV, l' is a backscattered Langmuir wave and s is the produced ion-acoustic wave. The velocity distribution of electrons becomes a so-called “bump-on-tail” distribution. This distribution leads to the excitation of Langmuir waves which drives the wave-wave interaction.

While this theory is able to explain the simultaneous enhancements in one or both the ion-lines, it does not require large field-aligned currents, nor does it require a large relative ion drift velocity. Due to the requirements of a low-energy precipitating electrons, it has difficulties explaining the Neials at lower altitudes, however.

4 Data retrieval from EISCAT

Incoherent scatter experiment data is publically available via the EISCAT database⁴. The format of the data, however, might not necessarily be used directly, but may require a processing step first. For this, the program Guisdap⁵ can be used. Guisdap is a multi-use program that is publically available via EISCAT. The program allows the raw data to be processed into a format that can be used directly by the program for automatic detection of Neials, which will be explained in more detail in section 6 in this thesis.

The EISCAT data is obtained from different radar systems, but each individual system may run various experiments, e.g. Tau0, Tau1 and Steffe. All the data that has been used in this thesis originates from the EISCAT database. The data of interest is the archived data, and it is required that it can be processed by Guisdap.

During the development of the program for automatic Neial detection, there were issues with data from the Steffe experiment. The issues were in processing the data using Guisdap, where the spectra were incomplete. Significant portions of the incoherent scatter spectra took the NaN (Not a Number) value. Experiments from the Tau0 experiment using the ESR 42m antenna could be processed in Guisdap without problems, and has been used throughout this thesis.

Preprocessing

When downloaded from the EISCAT database, the data is received as a compressed .tar file, which has to be extracted for use within Guisdap. This is a trivial step; most decompression programs can handle this format for a wide variety of operating systems. Guisdap can be pointed to this folder, and after assigning the basic settings for Guisdap, such as the integration period, which moments in time are relevant and various header data, the spectra can be generated. The additional information parameter that has been used in this thesis is

```
display_spectra=1;
analysis_range=[200:5:1000];
a_satch.do=0;
```

This tells Guisdap to generate spectra for each dump, where the spectra extends from 200 *km* to 1000 *km*, with a height resolution of 5 *km*. Guisdap will output all the preprocessed data in a folder specified by the user.

⁴ <http://www.eiscat.se/schedule>

⁵ <https://www.eiscat.se/groups/Documentation/UserGuides/GUISDAP>

5 Signature of Neials in EISCAT data

Raw EISCAT data come in pre-integrated dumps, where the height resolution and time resolution depends on the experiment itself. It is possible to post-integrate the experiments in order to obtain good measurements on the standard parameters such as electron density, temperature and bulk velocity, although that is of no interest in the procedures that will be discussed in this section.

There is one very important piece in the raw data that will be extensively used throughout this section, that being the actual spectra. Guisdap is used to generate these spectra from the dumps obtained from the experiments, and MatLab is the main platform used to process these spectra.

The spectra are given as a matrix of values, where each value corresponds to a given frequency in a given spectrum in that dump. The spectra themselves are stored along the first dimension, where the second dimension indicates which gate index the spectra are associated with. In addition to the spectra, the raw data contains a frequency matrix that associates a frequency to each cell in the spectra matrix. The data additionally contains a range vector, which associates an altitude with each spectrum in the spectra matrix. Other information include header information, such as the name of the experiment and the time at which the dump was obtained, the location where the experiment took place, as well as information about the geometry of the experiment, such as elevation and azimuth angle.

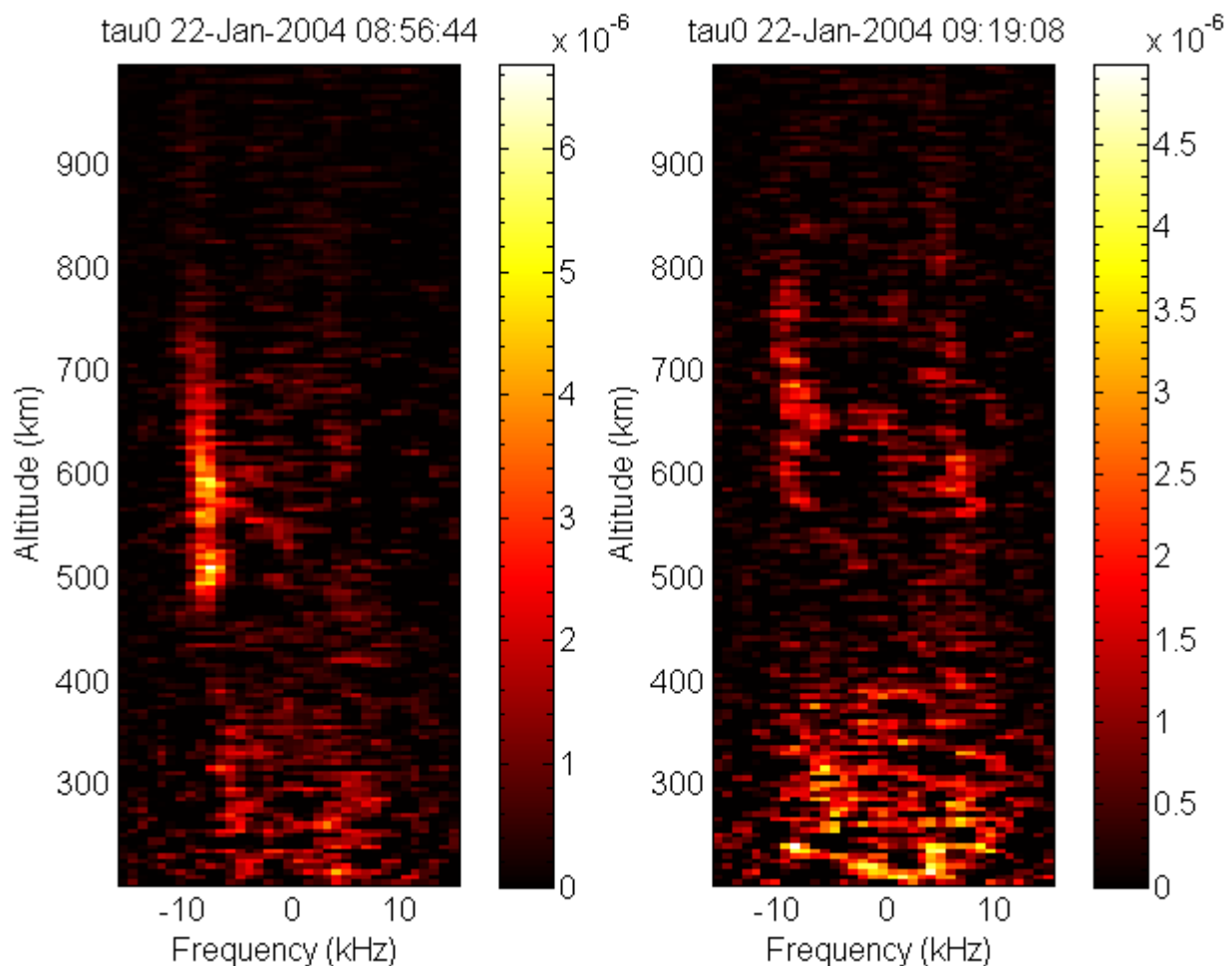


Figure 10: A couple of dumps from an experiment using the ESR 42m system have been plotted here. The magnitude (power received, in arbitrary units) is represented by the color bar. In both panels, a Neial can be spotted.

In order to determine whether the dump contains a Neial or not, however, it is enough to examine the spectra, the frequency and the range. In Figure 10 a couple of Neials have been depicted, where the enhancements in the ion-lines are spanning altitudes between 500 *km* and 700 *km* for the left panel, and between 600 *km* and 800 *km* for the right panel. Often it is simple to do perform a visual inspection of the spectra, but this is time-consuming and tedious. In order to have a computer spot Neials, it is necessary to classify a Neial, and a normal spectrum. There are several possible ways to do this, although in this thesis a select few methods will be examined.

5.1 Signature of satellites

Before going in depth of the methods, it is beneficial to look at the effect that satellites and other hard objects has on the incoherent scatter spectra. While the normal incoherent scatter is very faint, hard objects do not scatter incoherently. The net result is a strong, coherent echo. By looking at the power profile, a satellite will have a signature similar to what is displayed in Figure 11.

In the EISCAT data, this manifests itself as a localized spike, typically orders of magnitude greater than the regular signal. The sizes of these objects are not large, but in some cases the echo can blur out over a larger area, which is shown in Figure 12 in the lower-right panel. Typically these satellites can be found at altitudes above 500 *km*, although in some cases they can appear at lower altitudes.

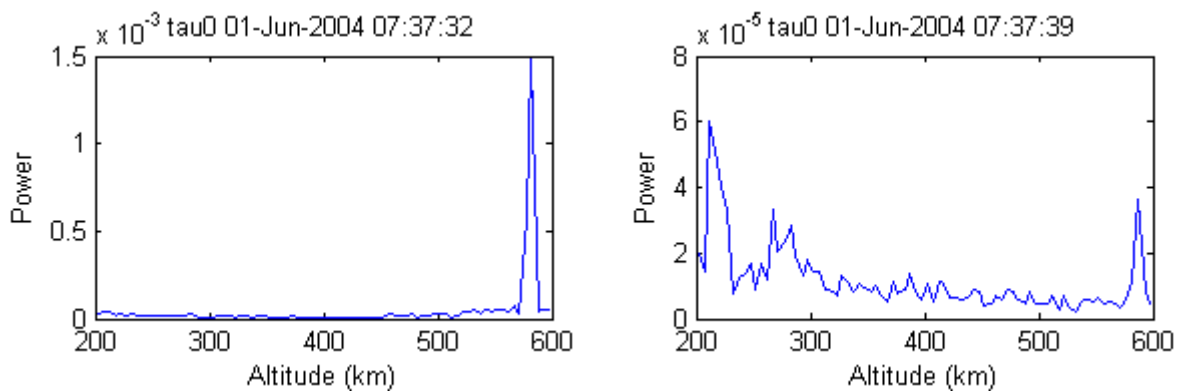


Figure 11: The power profile from a couple of dumps that contains a satellite. In the left panel it is clear that the echo from the satellite is significantly stronger. In the right panel, the echo from the satellite is weaker, located at just below 600 *km* altitude. The echo here is comparable to the magnitude of the regular signal. The power is given in arbitrary units.

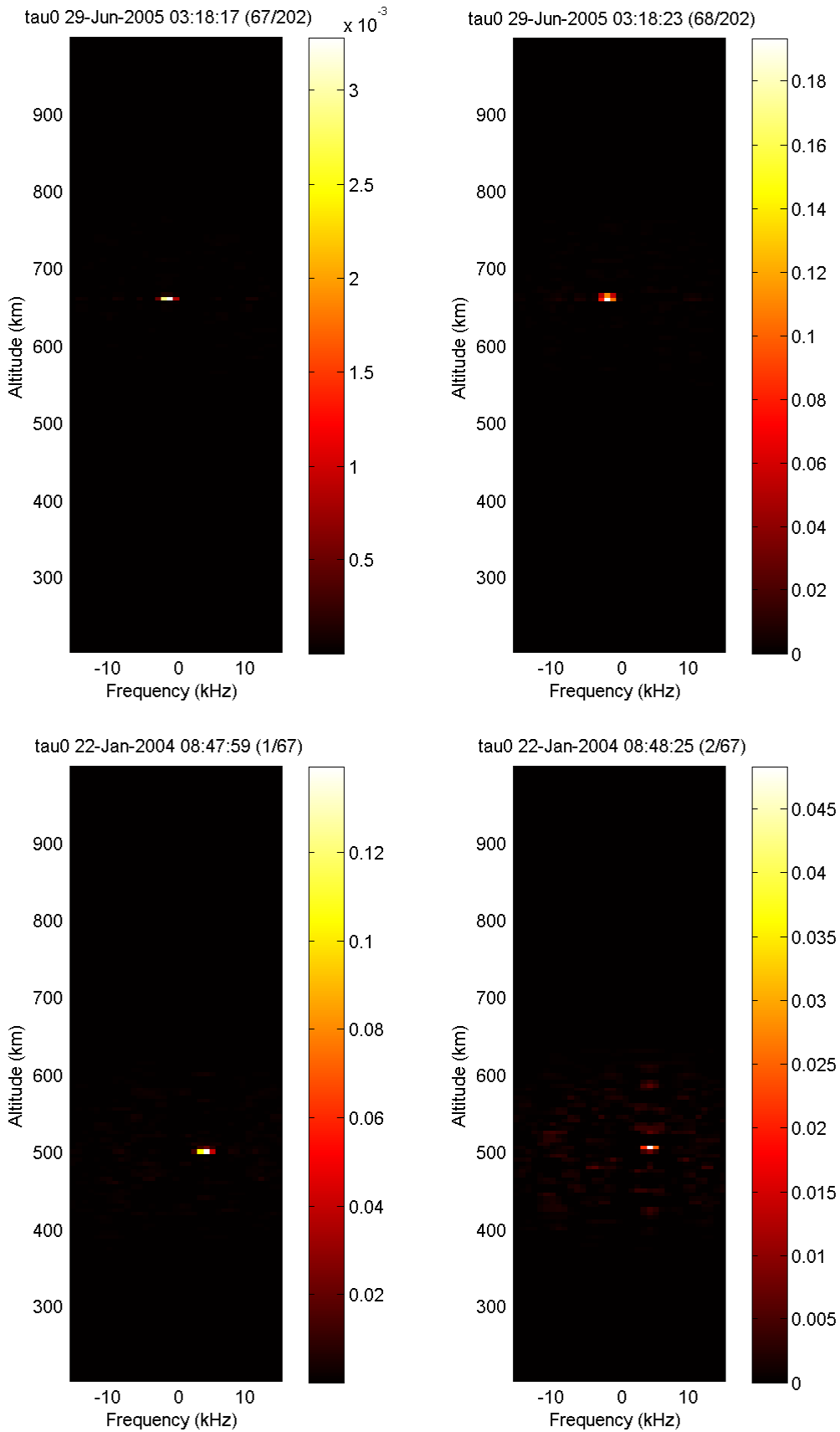


Figure 12: Example of four satellites. Note the additional noise in the vicinity of the satellite spikes. This additional noise is displayed clearly in the lower-right panel. This massive contribution from the satellite dwarfs the regular conditions, drowning them completely.

5.2 The histogram of the spectra

At first, it is tempting to attempt a somewhat simple method and perhaps a bit naïve method of detecting Neials. The idea is that during a Neial, the receiving antenna will detect a massive increase in the signal received, thus affecting the distribution of the received power. As a first thought, what does this distribution of apparent power look like? If taking all the power values in all the spectra and simply plotting them as a histogram, the result will be something that drops off exponentially. It is apparent that the signal from higher altitudes will be weaker, thus contributing only to the lower end of the histogram.

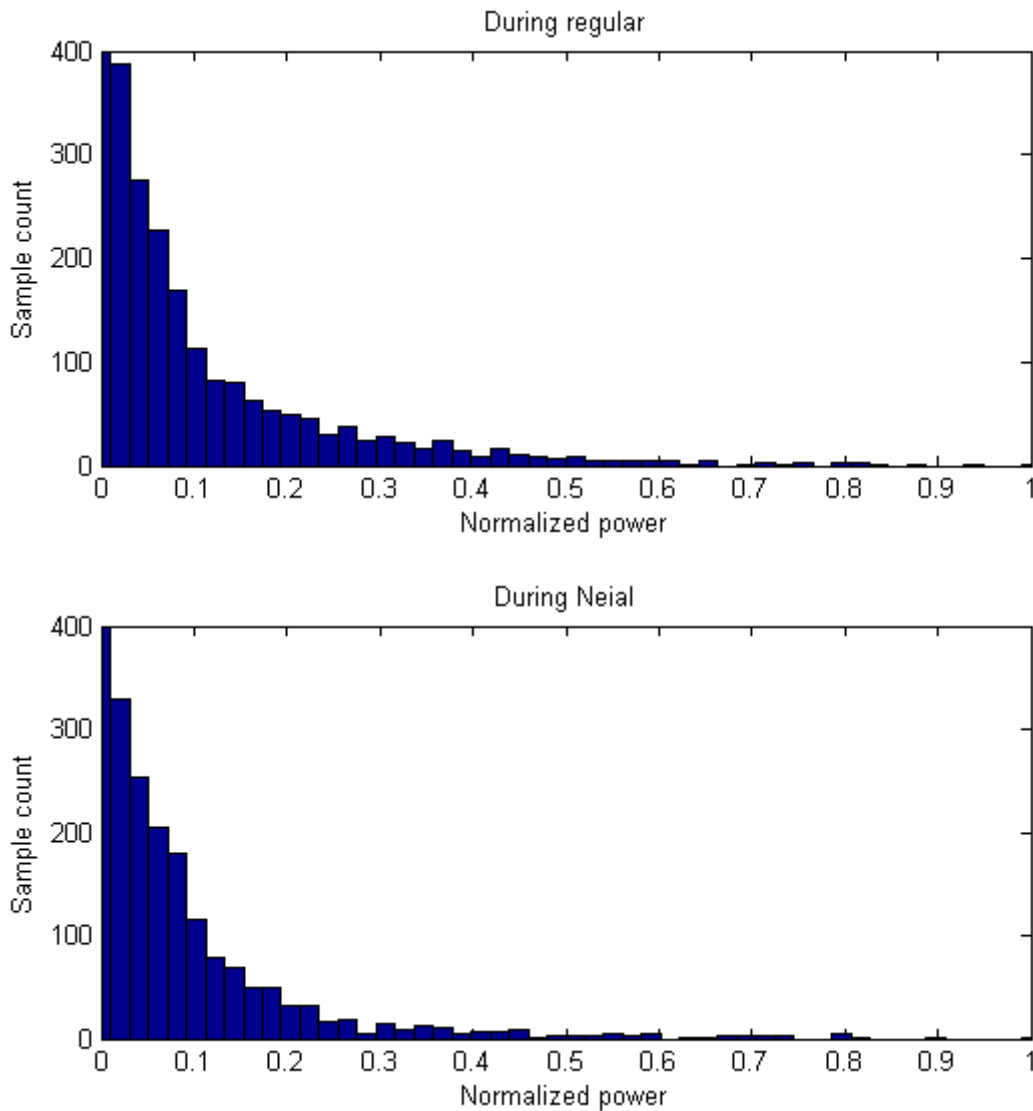


Figure 13: The distribution of powers for the whole spectrum during regular conditions and during a Neial. Both events are from June 1st, 2004, measured using the ESR fixed 42m antenna. The time of the regular situation is 07:30:55 UT, and the time of the Neial is 07:35:56 UT.

The effects Neials have on this distribution depend on the size and magnitude of the Neials. The strength of the Neial determines which section of the distribution it will affect, while the size of it determines how much of an overall effect it has. The Neial that has been depicted in Figure 13 was about normal in intensity. The net influence on the histogram is questionable, however, which suggests that the idea of examining the distribution need some modification.

Instead of normalizing the distribution by the maximum power of all the spectra, the next approach is to examine each spectrum separately, and normalize by the largest value in each spectrum. By plotting the values in a histogram this time, it becomes clear that the measured power values are rather evenly distributed in the regular case. The effects of a Neial become apparent in this situation. Since the bandwidth of a Neial is typically a small portion of the total spectrum bandwidth but contributes by a significant amount, it is expected that the majority of the power will be in the lower end of the distribution, while the contribution from a Neial will be in the upper end.

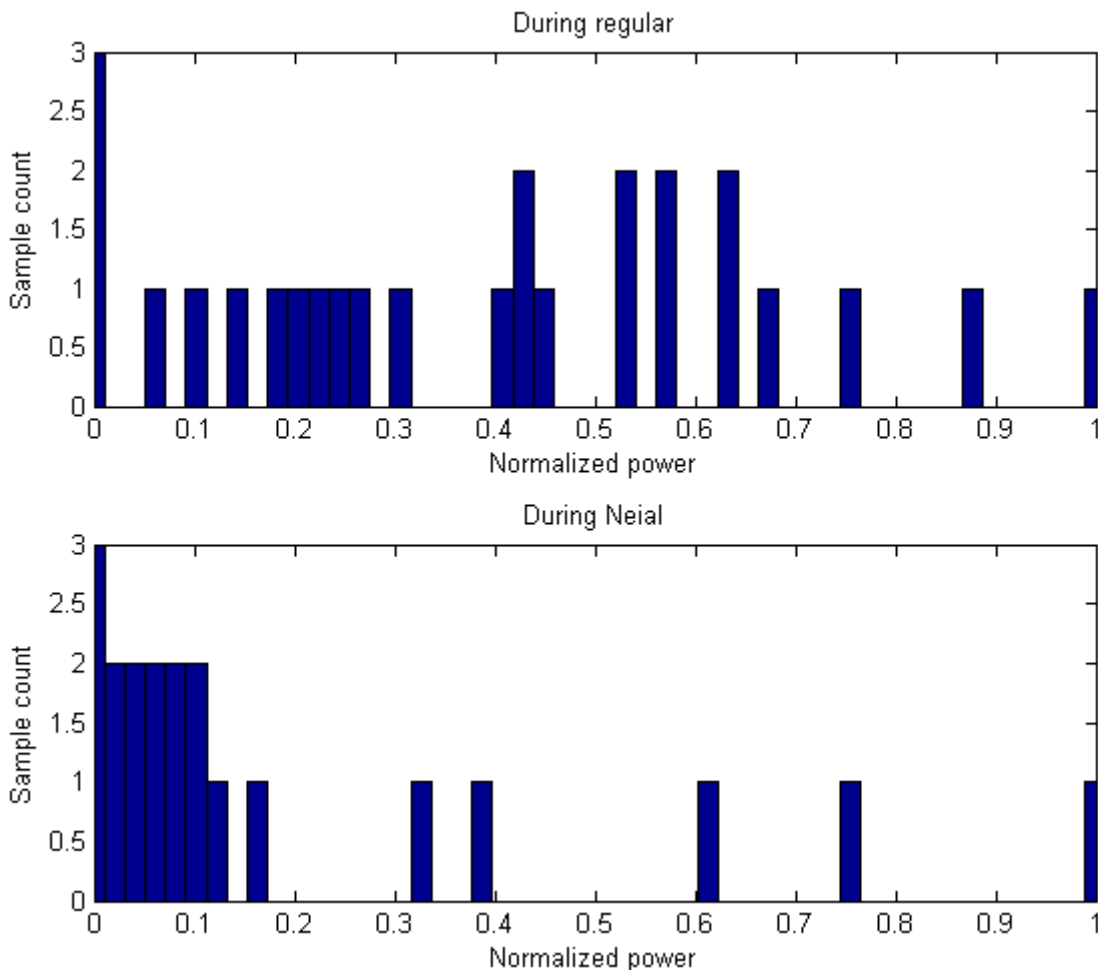


Figure 14: Histogram of the power distribution from two different spectra during the same conditions as show in Figure 13. The chosen altitude is roughly 510-515km. The distribution during regular conditions appears to be more evenly spread out than that in the case of the Neial.

When going through the spectra one spectrum at a time, it is easier to see a difference in the power distribution between normal conditions and the conditions during a Neial. As expected, the distribution of the power is clumped together in the lower end in the case of a Neial (See Figure 14, lower panel). When a Neial occurs, the apparent power is increased significantly, often on the order of a magnitude or more. When normalizing the spectrum, this forces the regular condition power values towards the lower brackets in the histogram, reserving the upper brackets for the contribution from the Neial.

The next step is to utilize this difference in distribution such that a computer can determine whether it has found a Neial or not. One aspect that is important to note is that the powers stored in the

spectra may, due to various systematical reasons, contain negative numbers. These values are considered as unphysical and clamped to zero for all intents and purposes.

In order to determine if there is a Neial in the spectrum, the spectra may be examined one spectrum at a time. For each altitude, the average normalized power value of the spectrum is evaluated after trimming out a certain amount of the upper and lower values. Represented mathematically,

$$\bar{x} = \frac{1}{(1 - \alpha - \beta)N} \sum_{i=\alpha N}^{(1-\beta)N} \vec{x}_i \quad (5-1)$$

where α and β is the percentage of how many of the lower and upper terms, respectively, that should be trimmed away, N is the number of elements before the trimming, and \vec{x} contains all the normalized power values, sorted from lowest to highest in numerical order. \vec{x}_i refers to the i -th element in \vec{x} . The altitude average is now said to be \bar{x} .

Once \bar{x} is known, the ratio \vec{x}_n/\bar{x} may be calculated for each element in \vec{x} . If this ratio is great enough, this altitude is thought of to contain a Neial. A problem with this approach is that it will trigger if there is sufficient amount of noise present, which can often be the case at lower altitudes or at the very high altitudes.

By requiring that multiple altitudes have to contain a Neial, this problem can be bypassed. If a sufficient amount of altitudes are thought of to contain a Neial, and these altitudes are in close proximity, this method will have concluded that it has found a Neial.

5.3 Spectral peak

When a Neial occurs, there will be an enhancement in one, or both, of the ion-acoustic shoulders. This suggests that a routine for automatically detecting them is to study the ratio of the two shoulders. Previous work (Ogawa et al., 2010) has shown that this is a viable approach.

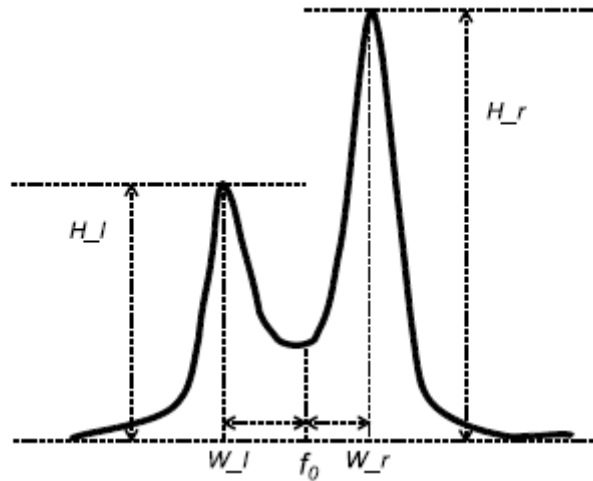


Figure 15: Illustration of the parameters used to identifying NEIALs. Here, f_0 is the transmitter frequency, H_l and H_r indicate the spectral peaks of the left and right ion lines respectively, W_l and W_r indicates the frequencies for the spectral peaks (from Ogawa et al., 2010)

The technique that was used (Ogawa et al., 2010) to detect Neials, was that for each altitude R above $200km$, a variable a was calculated according to equation (5-2).

$$a = \frac{H_l(R) - H_r(R)}{\text{Min}(H(R))} \quad (5-2)$$

Here, the left and right spectral peak is indicated by H_l and H_r , respectively, as shown in Figure 15. The difference between H_l and H_r was normalized by dividing by the minimum value of the peak at the same time, or one dump (6-s) before the time. In the equation, this is represented as $\text{Min}(H(R))$.

Then, if the parameter $|a| > 0.6$ in gates spanning 25 km or more, and if the frequency of the higher peak, W_l or W_r , was within 5 kHz in the same consecutive gates, the height profile of the spectra would be stored for future analysis.

In order to utilize the method outlined by Ogawa et al., however, there is an issue that must be considered. The process of extracting these peaks from the spectra is not as straight-forward as expected. There is one major concern that must be addressed – often the spectra are contaminated with noise, making the task of extracting meaningful information about the spectral peaks difficult if not impossible. Looking at Figure 16, the upper panel represents the normal conditions and displays difficulties of determining the location and height of the spectral peaks. In the case of a Neial (displayed in the lower panel of Figure 16), the contribution of noise is not typically relevant. The contribution from the Neial is significantly greater than that of the noise. The other peak, however, is not as easy to determine exactly, although it will not make a significant difference if the exact parameters of the peak is known.

The first approach to solve the noise issue may be to apply smoothing, trying to negate the effects of the noise. This does not solve the underlying problem, however, that the spectra do not always have a well-defined double-humped shape. In order to detect the peaks, it is required to define what a spectral peak is, regardless of how noisy the spectra are. It is well-known what a normal double-humped spectrum should look like (See Figure 5), which suggests that it is possible to bias the spectra to fit the general shape. By weighting each peak in the measured spectra by how close they are to where the expected peaks are, it is possible to calculate a reasonable guess for the actual spectral peaks' frequencies and magnitudes.

Given the spectral peak frequency $f_{L,R}$ for the left and right peak, respectively, the power associated with the peaks are $P_{L,R}$ for the left and right peak, respectively. Given any spectrum, the measured peaks are located at the frequencies f_0, f_1, \dots, f_N with the powers P_0, P_1, \dots, P_N associated with them. Suppose that the index n satisfy $f_n < 0$ and $f_{n+1} \geq 0$. Then, for the left peak,

$$f_L = \sum_{i=1}^n \alpha_i f_i, \quad P_L = \sum_{i=1}^n \alpha_i P_i \quad (5-3)$$

and

$$f_R = \sum_{i=n+1}^N \alpha_i f_i, \quad P_R = \sum_{i=n+1}^N \alpha_i P_i \quad (5-4)$$

for the right peak. Here, α_i represents the normalized weight of each peak and is a constant, and N the total number of peaks.

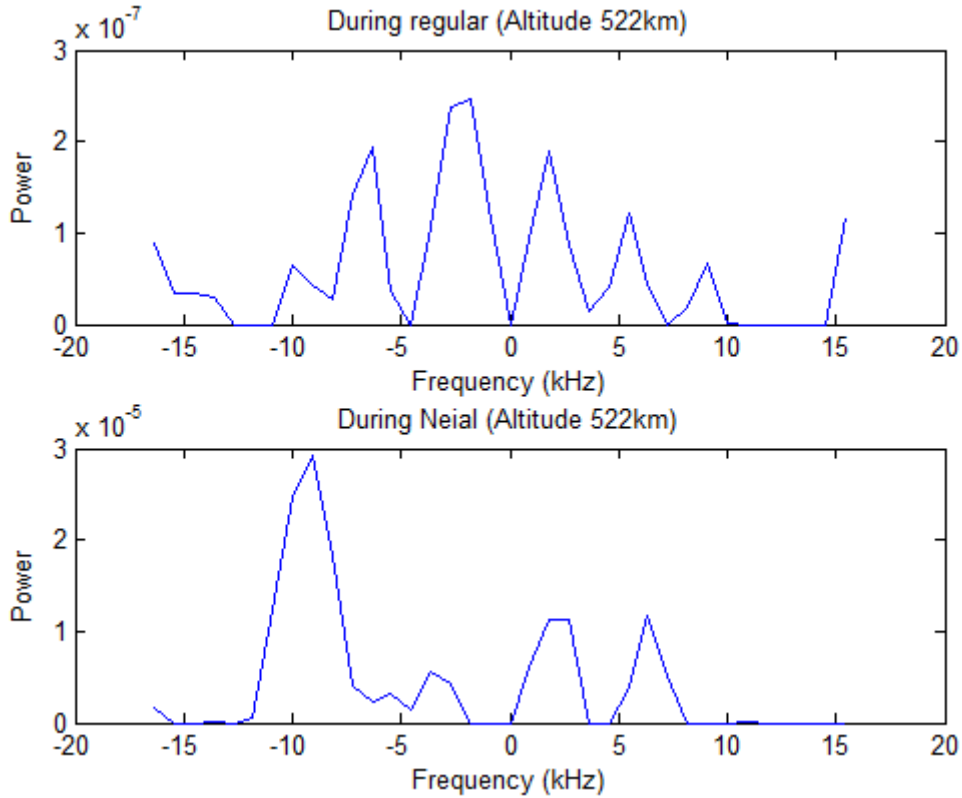


Figure 16: The spectrum for a certain height, illustrating the difficulties of detecting the spectrum spikes. The double-humped spectrum is ill-defined in these examples, although in the case of this Neial (lower half) it is easy to determine the downshifted spectral peak. The power is given in arbitrary units.

To calculate the weight of each peak, α_i , it is required to know the location of each peak. Finding all these peaks is trivial. Suppose that the powers are stored in an array, the peaks will then be located at all indexes where the received power is greater than both the neighboring values. The frequencies and magnitudes of these peaks can then be calculated from the indexes, yielding both f_i and P_i for index i .

Remembering back to the typical shape of the spectrum, there are three important regions. The first region is the valley between the spectral peaks. The second region is the spectral peaks themselves. The last region is the remainder of the frequency domain. It is desired that only the second region of the measured spectrum contributes, but this domain is often difficult or impossible to determine. Looking at Figure 16, in both cases it is quite difficult to determine where the peaks are, although in the case of a Neial one peak is typically easy to detect.

It might be worthwhile to approach this issue from another angle. Rather than trying to determine which region the measured peaks are associated with, it is possible to compute a weight for each peak on one simple rule. Measured peaks that are close to the expected frequencies for the spectral peaks are weighted more heavily than those that are further away or near the center valley.

Calculating this weight is fairly straight-forward. For the left and right side, respectively:

$$\alpha_i = \max\left(0, 1 - \frac{|f_i - \hat{f}_L|}{c}\right), \quad \alpha_i = \max\left(0, 1 - \frac{|f_i - \hat{f}_R|}{c}\right) \quad (5-5)$$

Here c is a constant with a magnitude of roughly 10 kHz and $\hat{f}_{L,R}$ represents the frequencies of the expected spectral peaks for the downshifted and upshifted lines, respectively. Typically these values would be $\pm 5\text{-}10 \text{ kHz}$. α_i has to be normalized, such that $\sum_{i=1}^n \alpha_i = 1$ and $\sum_{i=n+1}^N \alpha_i = 1$ is satisfied. By inserting equation (5-5) into (5-3) and (5-4), it is possible to fully determine $f_{L,R}$ and $P_{L,R}$. A few examples have been presented in Figure 17, where these values have been calculated from actual spectra.

While the results are not perfect, they yield a rough ballpark estimation as to what the spectral peaks might be in terms of magnitude, and at which frequency they may be located at. One weakness with this approach, however, is that if there is a peak near the center, and none near the expected frequencies, this approach breaks down.

In order to bypass this issue, a bias is introduced. Before running the peak detection, the spectrum is modulated slightly, to remove any peaks near the center, such that the index i that satisfies $f_i = 0$ also satisfies $P_i = 0$. This modulation can be represented as:

$$P'_i = P_i \min \left[1, \frac{|f_i|}{c} \right] \quad (5-6)$$

where c is a constant and has a value of roughly 5 kHz . The result of this modulation is illustrated in Figure 17, in the bottommost panel. The central peak has been removed through equation (5-6), before calculating the locations of the spectral peaks. By applying this operation, the spectral peak detection is able to position the peaks such that the Neial detection method discussed in this section is sufficiently accurate in general.

In common situations, displayed in the first and third panel in Figure 17, this approach is working to an acceptable degree. The locations of the spectral peaks and their magnitude are where they would be expected to be. In the case of the second panel, however, it is clear that the method is struggling with peaks near the center. The calculated power associated with the left spectral peak appears to be lower than expected in this case, as well as being slightly downshifted in frequency.

5.4 Power profile

It was stated in section 2.2 that one of the standard parameters that extracted from the spectra is the electron density, which is proportional to the total power in the spectrum. Under normal conditions this holds, but during Neials the analysis breaks down and the actual electron density cannot be determined.

If taking a series of spectra over a wide range of altitudes, and integrating over them, it is possible to plot a power profile. The actual electron density variation throughout the Earth's atmosphere is known (e.g. Figure 2). In the lower atmosphere there are very few free electrons, yielding a low density. The density increases with altitude and peaks in the E- and F-layers, then declines again in the upper altitudes.

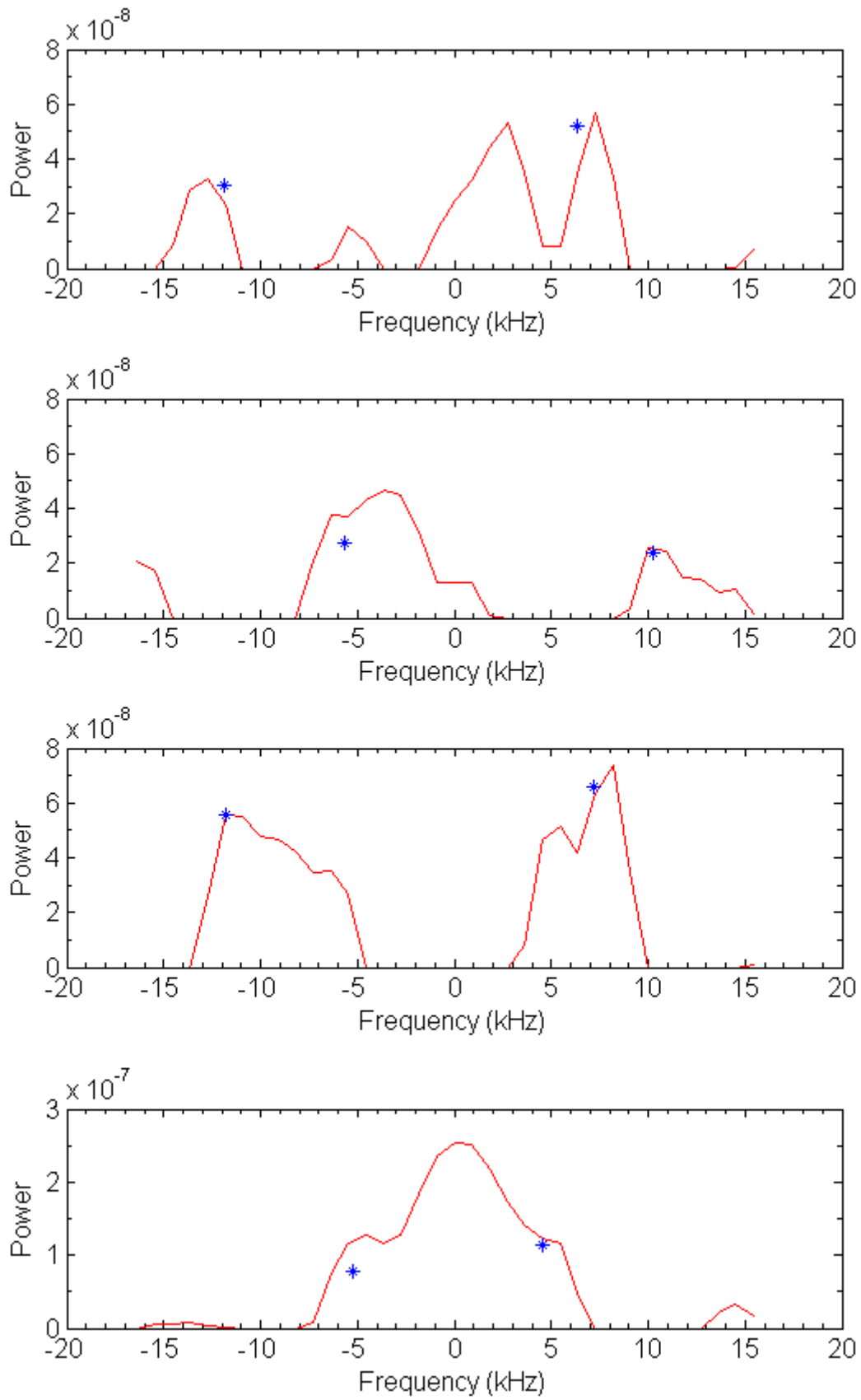


Figure 17: Peak detection from various spectra. The star markers represent the computed values for f_L and f_R , with the associated powers P_L and P_R , respectively. The power is given in arbitrary units.

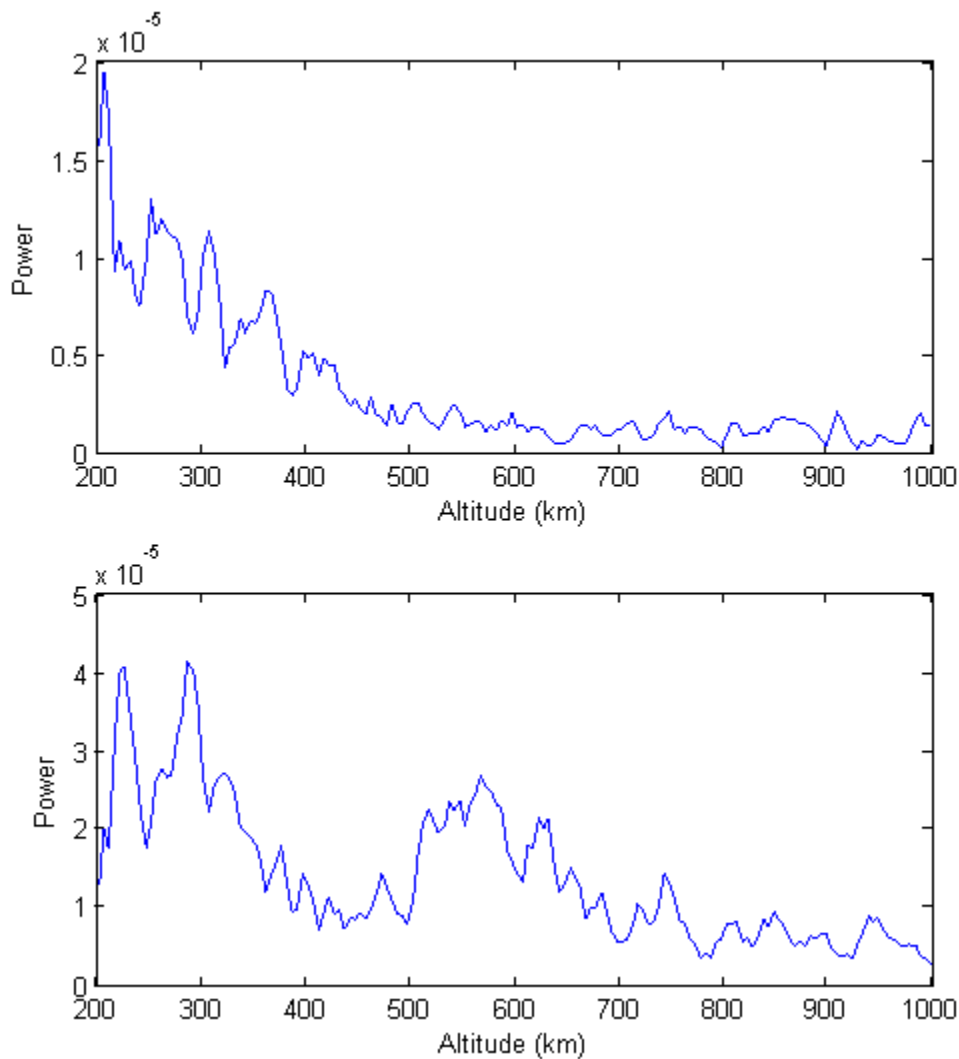


Figure 18: The power profile from two different times, where the upper panel is from regular conditions and the lower panel is from a Neial. It is clear that there is a significant enhancement in the power profile in the altitudes from about 500 km to roughly 700 km, which is a typical signature of Neials. Note that the scaling of the y-axis is different between the two panels. The power is given in arbitrary units.

During regular conditions, it is expected that this electron density profile will be reflected in the incoherent scatter spectra. Examining various spectra, this is what can be observed. During a Neial, there is expected to be a massive contribution of power in the signal. This can be seen in Figure 18 at an altitude of about 500-700 km.

In order to detect whether a Neial is present in this power profile or not, it is possible to try to model the profile with an exponential function. This is a relatively decent approximation for the upper altitudes, although this approach will be inappropriate at altitudes lower than 250-300 km, usually, as the electron density decreases drastically below the F-layer.

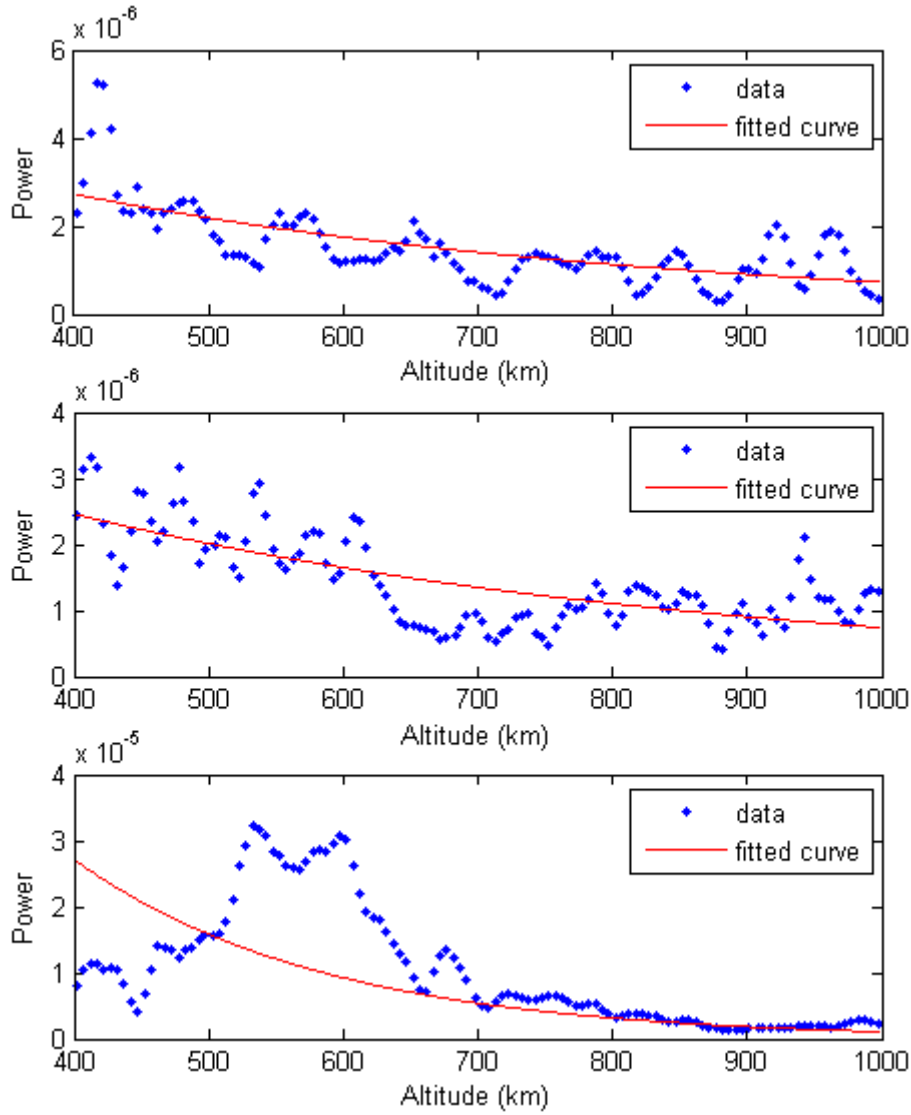


Figure 19: A few situations where an exponential curve has been fitted to the data. In the last panel, the curve is ill-fitting, which is typically the case for Neials, satellites or system errors. Note that the scaling of the y-axis is different between the three panels.

In order to measure how well a function f is fitted to the data, the deviation s can be defined as:

$$s^2 = \frac{1}{N-1} \sum_{i=1}^N (P[i] - f[i])^2 \quad (5-7)$$

The power profile is stored as an array P , where $P[i]$ is the i th element of the array, and f is the fitted curve function. N is the length of the power profile array.

In the regular case, once an exponential function has been fitted to the data, it is expected that the standard deviation should be quite low, whereas in the case of a Neial or other forms of anomalies, the standard deviation will be significantly higher. This is indeed what can be observed when computing the deviations from the data displayed in Figure 19; the deviation for the case of a Neial is typically an order of magnitude larger than that of the regular situations, sometimes several orders of magnitudes greater.

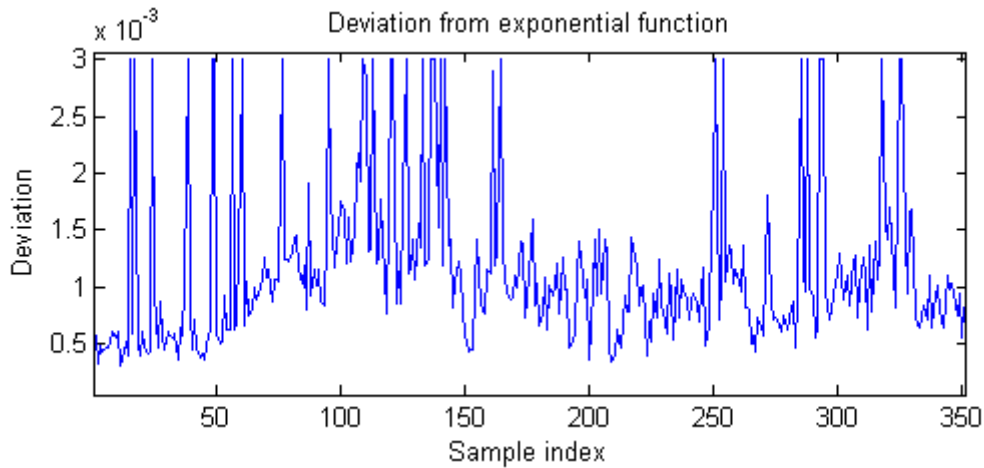


Figure 20: The deviation calculated from over 350 different power profiles over 22nd January, 2004, using the ESR 42m antenna, from roughly 08:45 UT to 10:00 UT. Note that the regular level is roughly at a magnitude of $1.5 \cdot 10^{-3}$ or less. The peaks in this graph are due to satellites, Neials or systematical errors. The deviations due to satellites and Neials are typically a few orders of magnitude greater than that of regular conditions. Values are clamped to $3 \cdot 10^{-3}$ here.

In the situation where the deviation is too significant, $s > 2 \cdot 10^{-3}$ (given in arbitrary units obtained from the EISCAT system), it can be said that a potential Neial has been found.

A weakness of this approach, however, is that it easily captures satellites, which typically yields a deviation that is sometimes orders of magnitudes greater than that of Neials. In order to remove these satellites, it is possible to apply a filter that removes noisy spikes from the data. Satellites are typically not large in height. That is, the effect they have on the spectra is well localized within a small span of altitude (typically less than 20 km), whereas Neials, which are the relevant structures, are typically wider in height, spanning a larger range of altitudes.

The filtered array may be represented as

$$P'[n] = \begin{cases} P[n] & \frac{P[n]}{\min(P[n-w], P[n+w])} < r \\ \frac{1}{2}(P[n-w] + P[n+w]) & \text{otherwise} \end{cases} \quad (5-8)$$

where r is a threshold value, w indicates some width and P' is the resulting array. For r , values near 10 works decently, as satellite echoes are strong and natural fluctuations or fluctuations due to noise are not sufficient to be triggered by this threshold. w would typically be set to a value that is equivalent to a few km.

An issue with this approach to remove satellites, however, is that the signal contribution from satellites is not always this simple. While certain contributions may be removed with ease, such as displayed in Figure 21, it is not always that simple. Turning the attention to Figure 22, even if the spike due to the satellite was removed, the sidelobes of the spike is still enough to drown out the wanted signals. While the method is good enough to remove the contribution from minor satellites and other minor hard objects, it will still fail if the echo from the object is sufficiently massive.

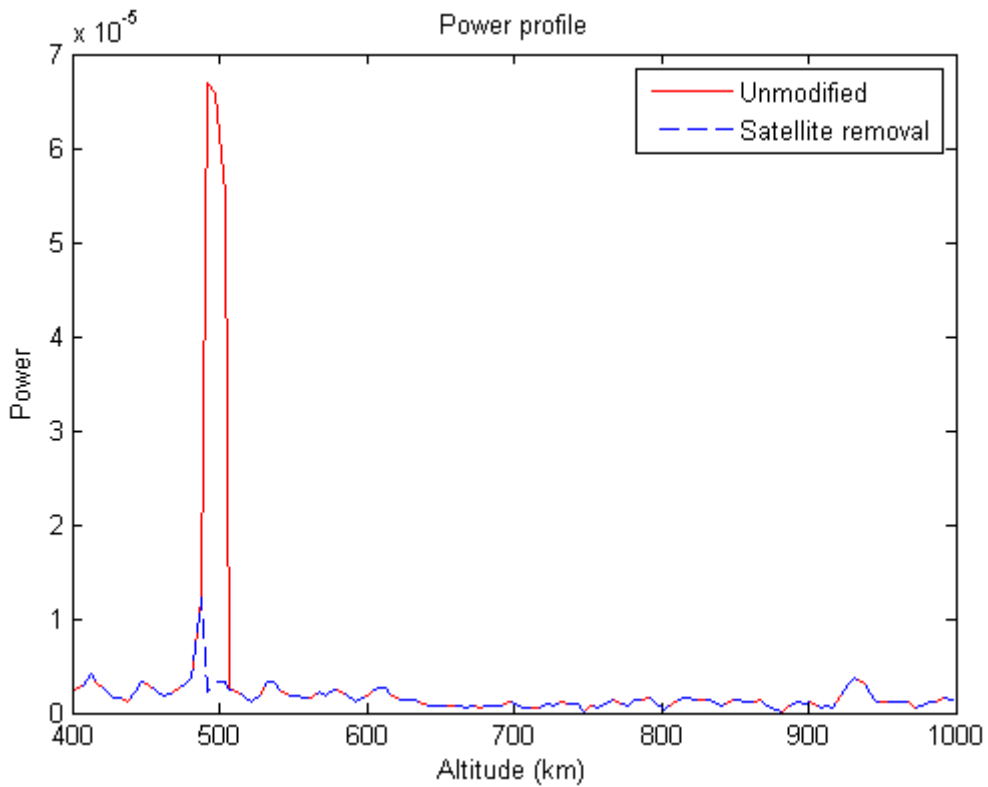


Figure 21: A power profile that has been contaminated with a satellite spike. After applying the filter as described by equation (5-8), the satellite echo is significantly reduced. Note the unique signature of the satellite in the power profile, which makes it relatively easy to remove these unwanted contributions. The power is given in arbitrary units.

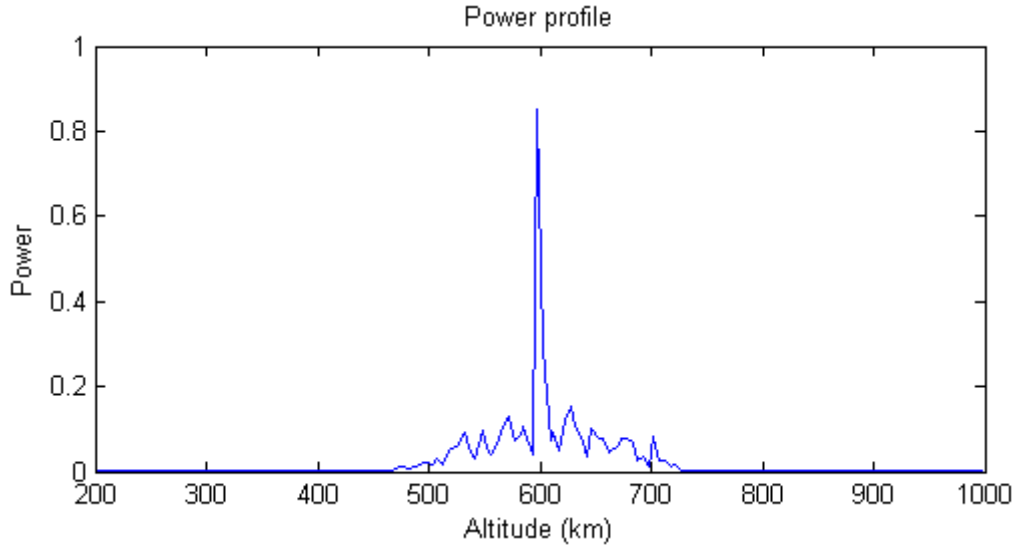


Figure 22: A typical very strong satellite echo, which bleeds out over to other nearby slices of altitude. Even if the satellite spike is removed, the net effect of the satellite still drowns out the background signal. The power is given in arbitrary units.

6 Automatic detection of Neials in EISCAT data

All the tools for detecting Neials in the data have now been developed, and the data is on a format that is easy to work with. What follows next, is the program that will apply the various tools to the data. In this section, these tools will be translated to algorithms that take in one dump, processes it and then tells whether a Neial was found in that dump or not.

6.1 Algorithms

Histogram

As discussed in section 5.2, the histogram will be examined for each slice of altitude. The algorithm starts from one edge (in this implementation, from the lower altitudes), and traverses the entire dump one spectrum at a time. Each spectrum is examined individually, independent of each other. The results from each examination are then used to determine if the dump contains a Neial or not. If enough spectra within 25 km were considered to contain a Neial, the entire dump would be considered to contain a Neial.

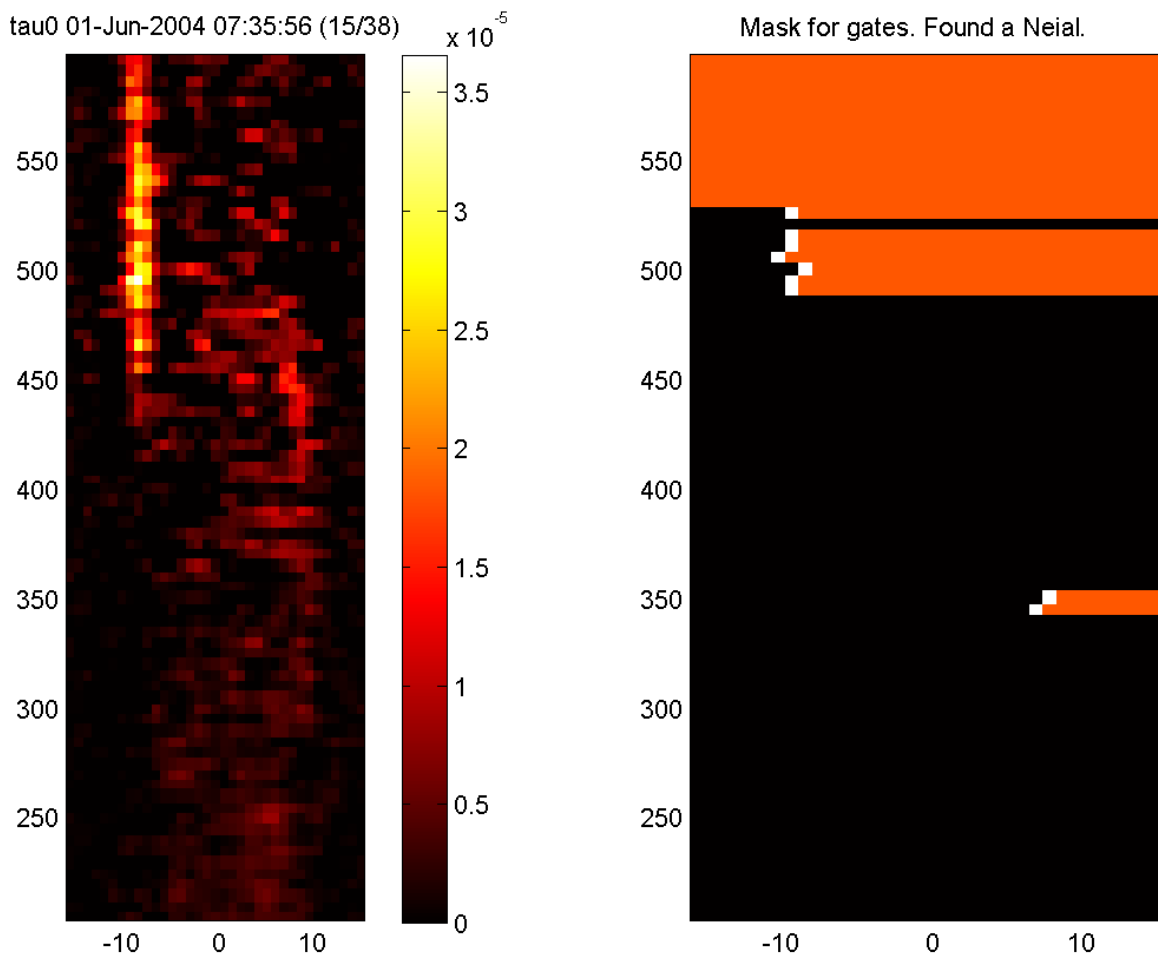


Figure 23: A Neial detected by the ESR fixed 42m antenna. Note the random contribution near the middle in the rightmost figure, where the algorithm has incorrectly determined, due to noise, that a couple spectra contained a Neial. The x-axis is the frequency (in KHz) and the y-axis is altitude (in km).

The process has been illustrated in the right panel in Figure 23. The algorithm traverses the entire dump, one spectrum at a time. When the algorithm finds nothing that it considers to be a Neial, it marks the entire spectrum as void and moves on to the next spectrum (represented with a black

color). When it finds values that satisfy the conditions for a Neial, it marks the position in the spectrum and stores it (represented with a white color), ignoring the rest of the spectrum and moves on to the next spectrum. Once enough spectra satisfy the conditions, the algorithm terminates and announces that it found a Neial.

In this implementation, the ratio required for the ratio \vec{x}_n/\bar{x} defined in equation (5-1) was set to 8, and the number of altitudes needed to contain a Neial was set to be 6. The ratio of values trimmed away was $\alpha = 0.65$ and $\beta = 0.25$. This allowed the algorithm to detect Neials decently, while avoiding false positives due to noise and most satellites. In section 7.2, a small change which improved the accuracy of the method significantly will be discussed.

Spectral peak ratio

The method used by Ogawa et al. (2010) is slightly different from the approach used in this thesis. In the approach defined in this thesis, the parameter a , which is calculated according to equation (5-2), is not normalized by dividing by the minimum value of the peak at the same time. Instead, it is normalized by dividing by the largest value from the current, or the previous spectrum, whichever is larger. This approach avoids several divide-by-zero issues, which leads to a poorly defined parameter a . Additionally, it has been observed that when normalizing by the minimum value of the peak, the parameter a was significantly larger in the presence of noise, especially in the cases where either the upshifted or downshifted spectral peak could not be located, or was too contaminated with noise. A consequence of this was that the algorithm reported too many false positives.

Another difference to the method used by Ogawa et al. (2010) is the lack of comparison with the previous dump. The method defined in this thesis does not make the assumption that each dump is within a few seconds of the previous dump, which would imply a small time difference between each dump. It is conceivable that the time between each dump is 120 s or more, which is ample time for the ionospheric conditions to change between each dump. It is also conceivable that certain dumps may be missing in the data that is being processed due to various system errors, which would also cause significant issues, if comparing to the previous dump.

The spectral peak algorithm defined in this thesis examines each spectrum on its own. It will then take the results from each spectrum in order to determine if a Neial has been found, similar to the algorithm used to detect Neials from the spectrum histograms. The algorithm traverses the dump, one spectrum at a time, from the lower altitudes to the upper altitudes. Whenever a spectrum is determined to qualify for a Neial, it is kept track of and stored in a list. When the list contains enough entries that are within 25 km of each other, and the peaks are within 5 kHz of each other, the dump is said to contain a Neial.

This algorithm has some important advantages over the algorithm that examines the histogram. First and foremost, it is not as prone to failing due to the presence of noise. It is known that one or both the spectral peaks are amplified during a Neial, which makes the amplified peak or peaks relatively easy to detect using a computer. Typically, noise may be able to result in a parameter $a > 0.6$, however, this is very unlikely to happen to every spectrum spanning 25 km. As shown in Figure 24, on the lower right panel, there are two false positives reporting from about 350 km altitude, and one at just below 400 km, although this is not enough to qualify as a Neial.

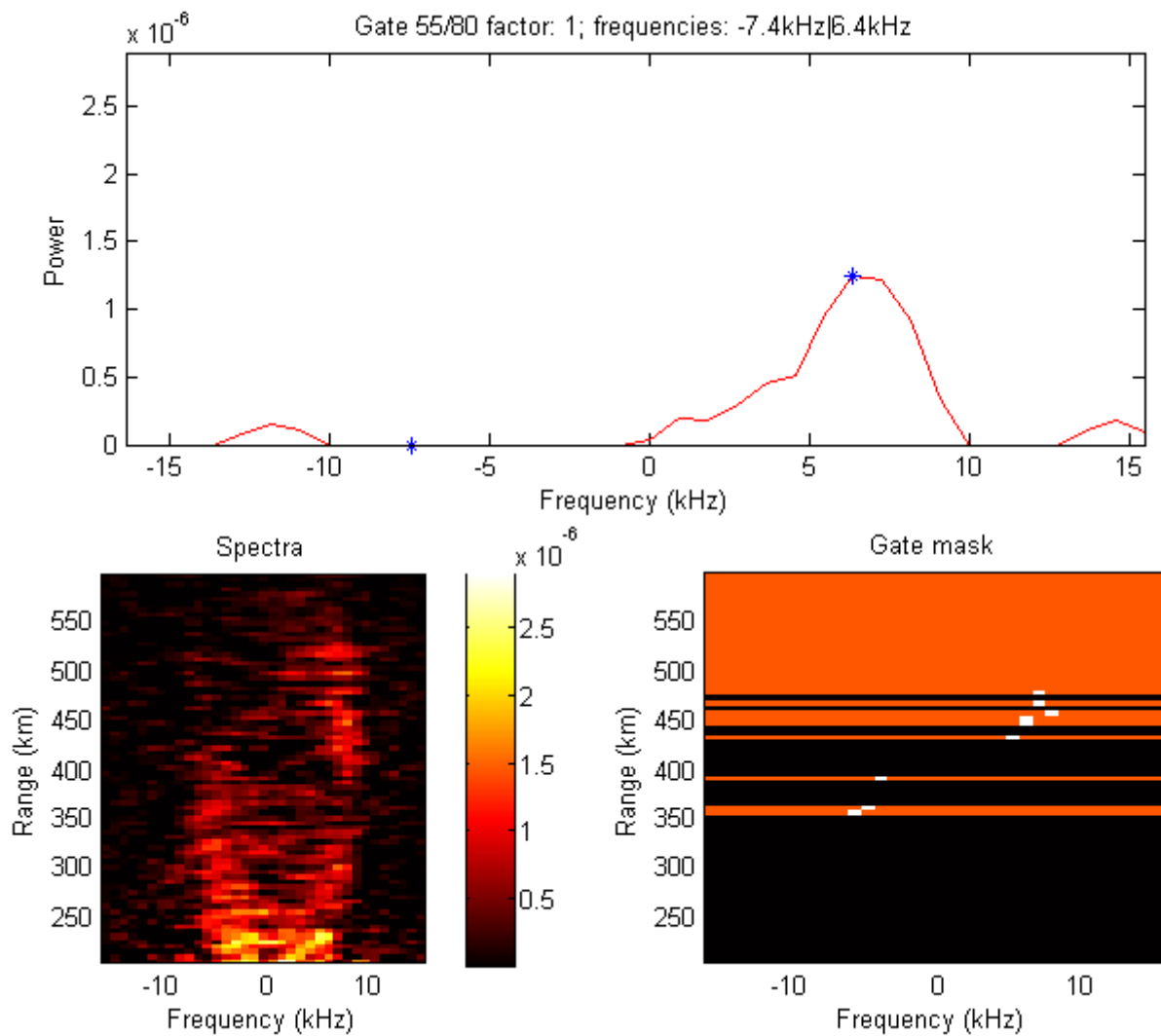


Figure 24: The peak algorithm examines each spectrum individually, first locating the spectral peaks, then calculating the parameter α . For each altitude where $\alpha > 0.6$, the location of the peak and altitude is stored (marked as white in the lower-right panel).

One quite useful advantages provided by this algorithm is that it also ignores most satellites and other hard objects. Such objects are typically small, not spanning many gates, thus they do not immediately qualify as a potential Neial, despite standing out in the spectra as a massive enhancement in one side of the spectrum.

Power profile

Whereas the previous two algorithms consider only each individual spectrum one by one, the power profile algorithm integrates all the spectra. The integration is performed over the frequency, yielding the total power as function of altitude.

At this point, it is possible to use regression to model the power profile. In order to simplify this problem, the algorithm trims away all data that is associated with an altitude lower than 400 km. This removes the need to take into consideration the shape of the electron density curve at altitudes corresponding to the E- and F-layers. An obvious downside to this approach, however, is that if a

Neial occurs at lower altitudes than that, this algorithm will never be able to detect that. By improving the model for the electron density, however, this issue can be alleviated.

Turning the attention to Figure 25, this approach can be seen. The upper and lower panels are regular conditions, where the standard deviation is about an order of magnitude less than that of the middle panel, which does contain a Neial. In the former case, the exponential function is a decent enough approximation, and in the latter case, the exponential function is a very poor approximation.

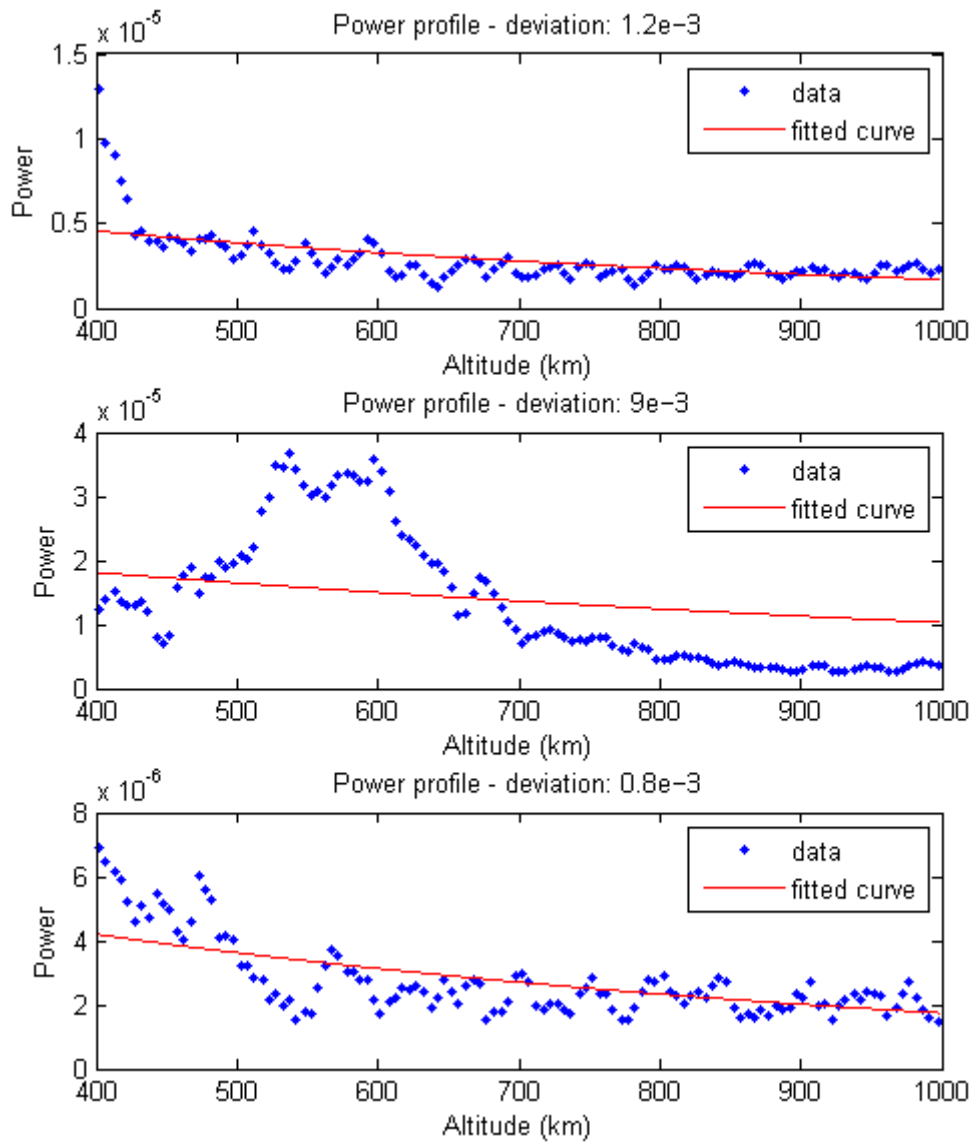


Figure 25: A few power profiles that have an exponential function fitted to them. The middle panel illustrates an exponential function that is clearly not fitting, thus it qualify as a Neial. Note the difference in scale between the panels. The power is given in arbitrary units.

7 Results

Three different methods of detecting Neials in EISCAT data has been discussed in this thesis. It is not yet clear how these methods will perform on actual data, if they will be able to accurately select relevant moments in time and ignore uninteresting moments.

There is also a question of which section the various methods can be applied to. That is, which regions of altitude they are valid at and which altitudes they perform best at. It is conceivable that the accuracy varies as a function of altitude as well, as noise may be more prominent at lower altitudes, as well as very high altitudes. It remains to determine how well the various methods cope with noise as well.

There will be many different satellites and hard objects showing up in the spectra, all of them being uninteresting; it is desired that dumps containing satellites are omitted, even if they contain a signature of Neials. Certain methods may be more efficient at ignoring such hard objects than others.

7.1 Establishing baseline

In order to determine how well the various methods perform, it is essential to have a baseline to compare their performance with. This baseline is established by generating a series of images depicting spectra from various moments in time where Neials are known to be found. These images are then examined by visual inspection, looking for signatures of Neials.

One moment that was chosen as a baseline, was June 1st, 2004, from approximately 07:30:00 UT to 08:45:00 UT, using the ESR 42m antenna. Going through the data at this moment resulted in five very clear Neials and three potential Neials (although two of these incidences were very faint). Some of these dumps are shown in Figure 26 and Figure 27. In total, there were 348 dumps obtained from this time period. Roughly 2.3% of the dumps in this period were classified as containing Neials, by visual inspection. The altitude range of the dataset is spanning from 200 *km* to 600 *km*, thus there is a possibility that Neials from higher altitudes are not captured in this case.

Another moment that was chosen was January 22nd, 2004, from approximately 08:45:00 UT to 10:00:00 UT, also using the ESR 42m antenna. During this time, about 30 decently clear to very clear Neials could be found through visual inspection. Another 14 potential Neials were also spotted, although many of them quite faint. Some of the Neials found here are shown in Figure 27 and Figure 28. In total, 352 dumps were obtained from this time period. In this case, roughly 12.5% of the dumps were classified by visual inspection to contain a Neial. This is in good agreement with the numbers reported by Lunde et al. (2007) from roughly the same moment in time. The altitude range for the dataset is spanning from 200 *km* to 1000 *km* in this case.

A couple of tests for the various algorithms can be defined. The first test will be the first moment (June 1st, 2004), and the second test the second moment (January 22nd, 2004). The algorithms will be applied to these datasets. The dumps they return will then be compared to what has been found by visual inspection.

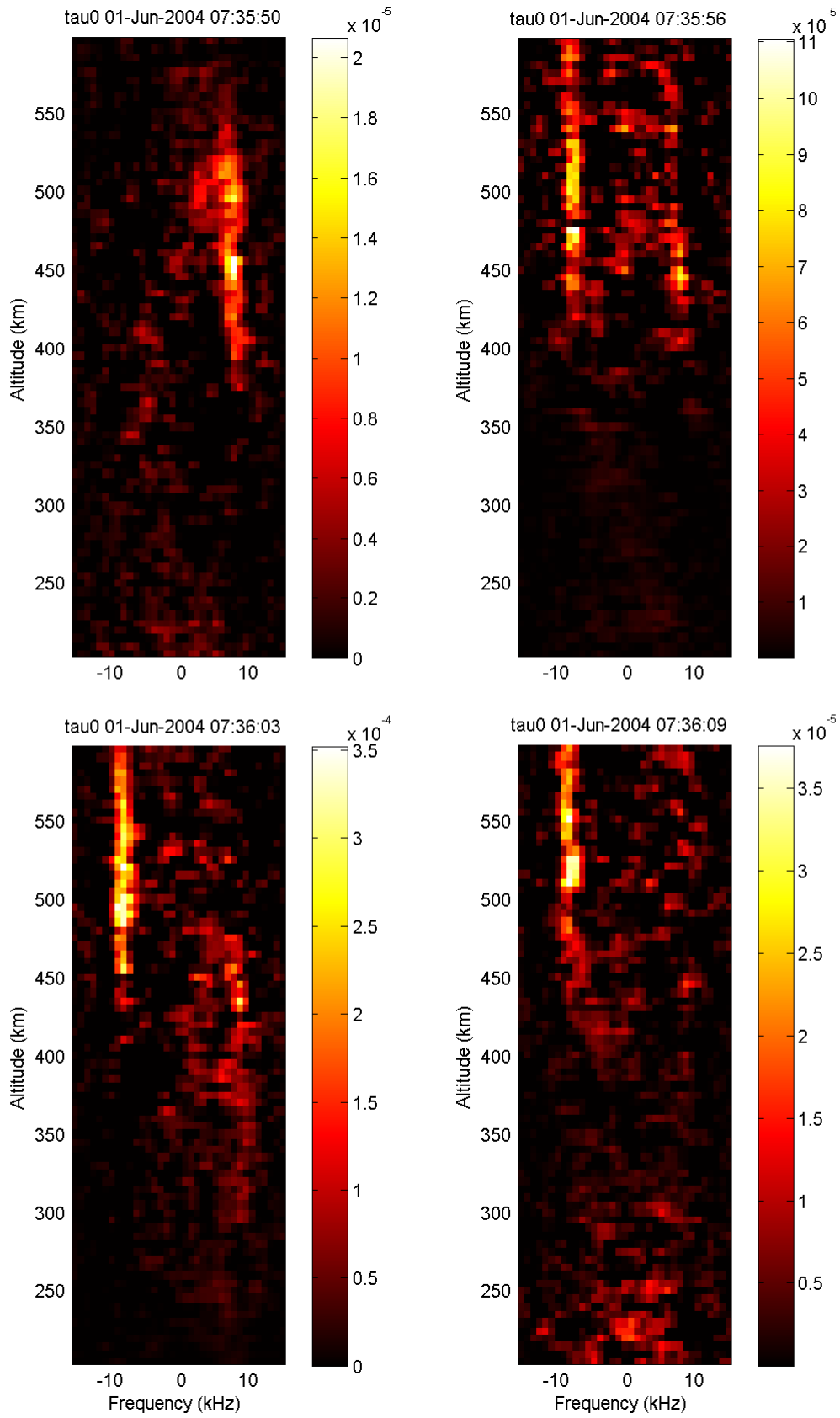


Figure 26: Four Neals that has been found by manually examining the spectra obtained from the ESR 42m antenna.

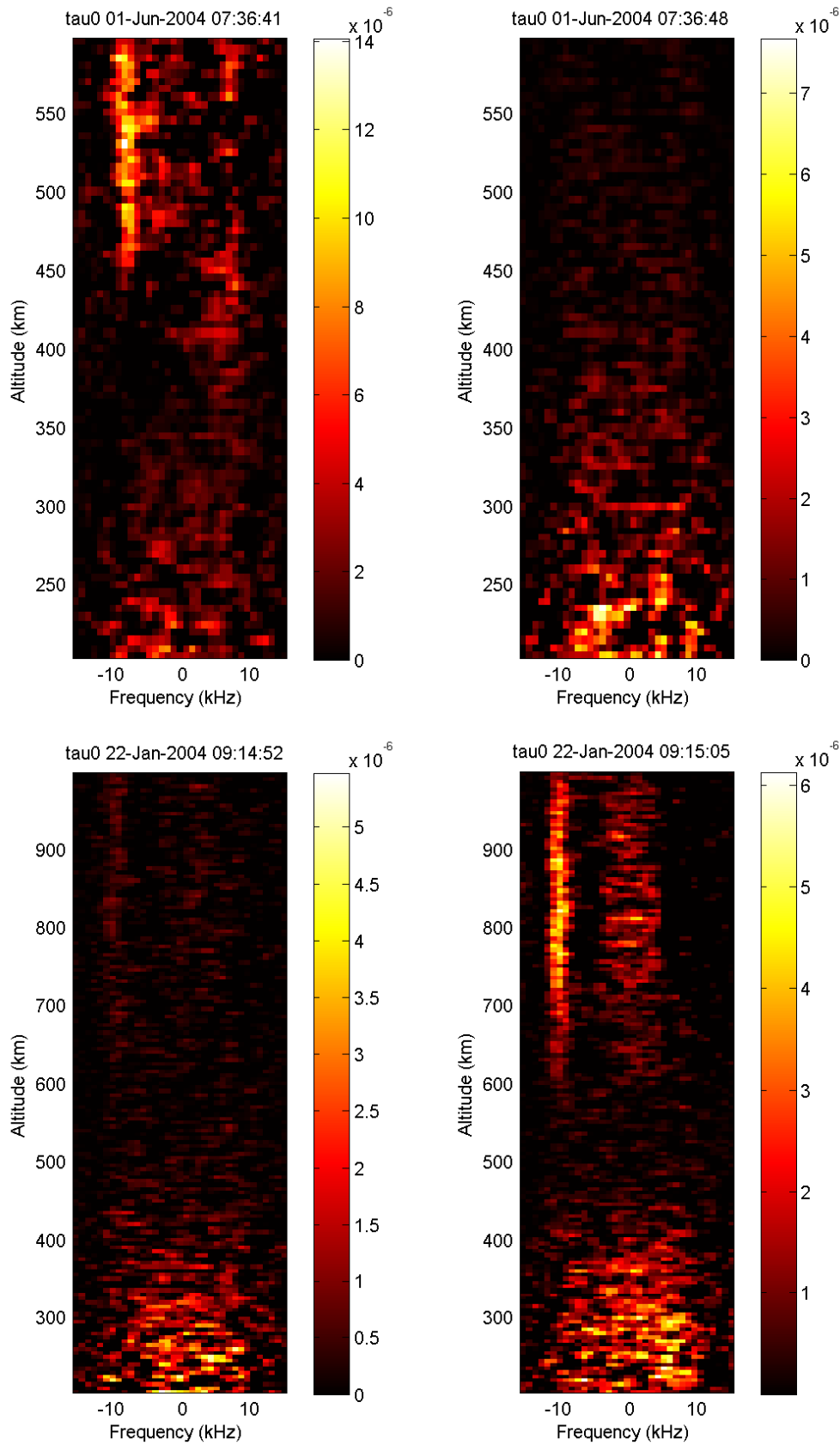


Figure 27: Two Neials that has been found by manually examining the spectra obtained from the ESR 42m antenna. The upper right panel side does not contain a Neial. The lower left panel may be a Neial, although it is very faint and contaminated with noise.

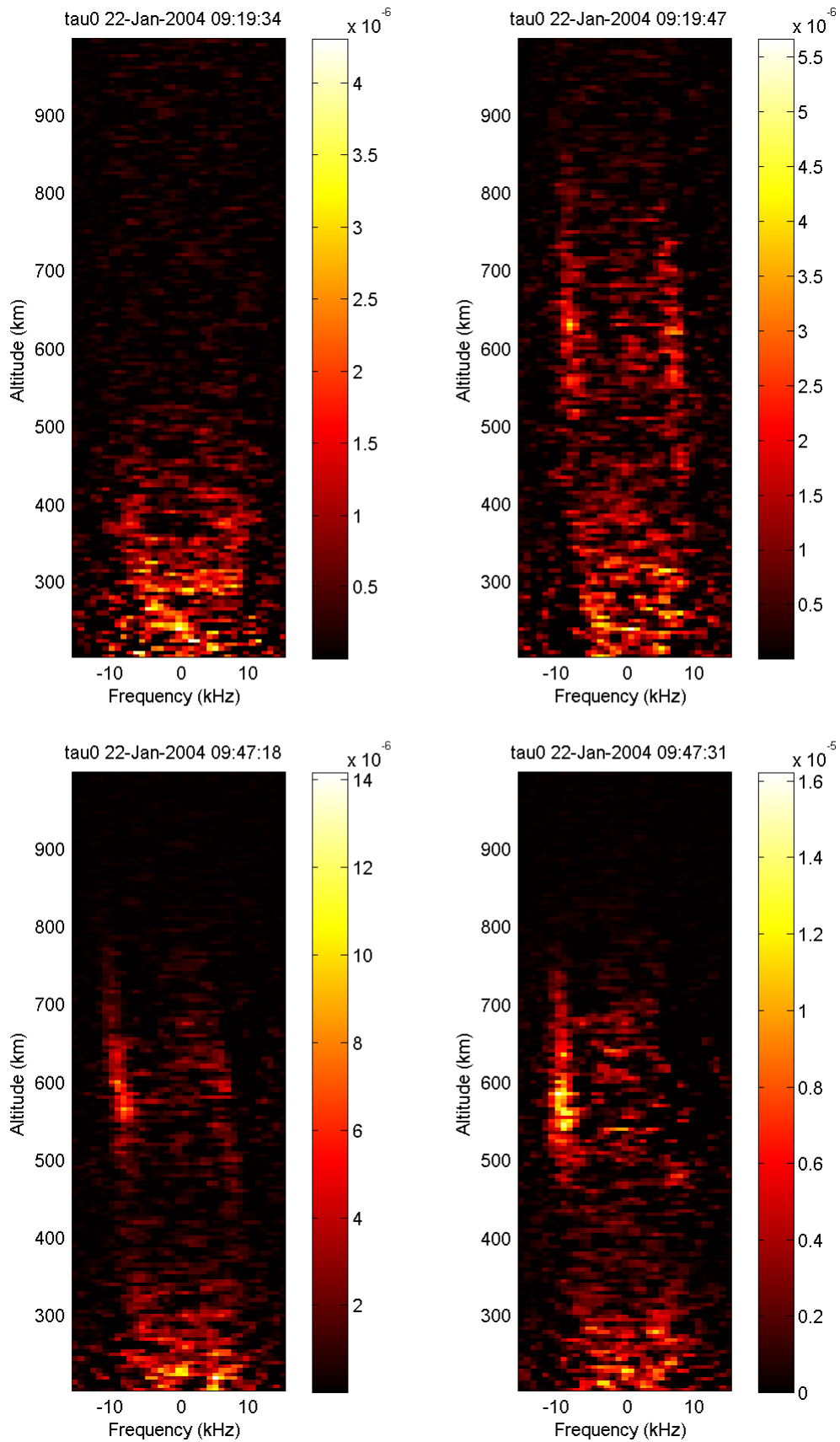


Figure 28: Three Neials that has been found by manually examining the spectra obtained from the ESR 42m antenna. The upper left panel does not contain a Neial. In the upper right panel, a simultaneous enhancement can be seen.

7.2 Algorithm performance

Histogram

While examining the histogram of the spectra is by far the fastest method of the three, it becomes quite apparent that it is not nearly as accurate as it needs to be. By using this method on the same data which was used for benchmarking, while it performs reasonably well on the first test, it fails significantly on the second test.

During the first test, this method reported five out of 348 dumps to be a Neial. Of these five dumps, four were actually Neials, and the last dump was a satellite. Considering that out of these 348 dumps five were actual Neials (plus three weak potential Neials), this is a very decent result.

During the second test, however, the method reported 91 out of 352 dumps to be a Neial. Of these 91 dumps, only a mere 14 were actual Neials, and 10 were satellites. An astounding 61 were false positives. 6 of dumps could have been Neials, but were quite faint. The actual Neial count in the same dataset is closer to 40, which suggests that the method might be too naïve to be used in practice.

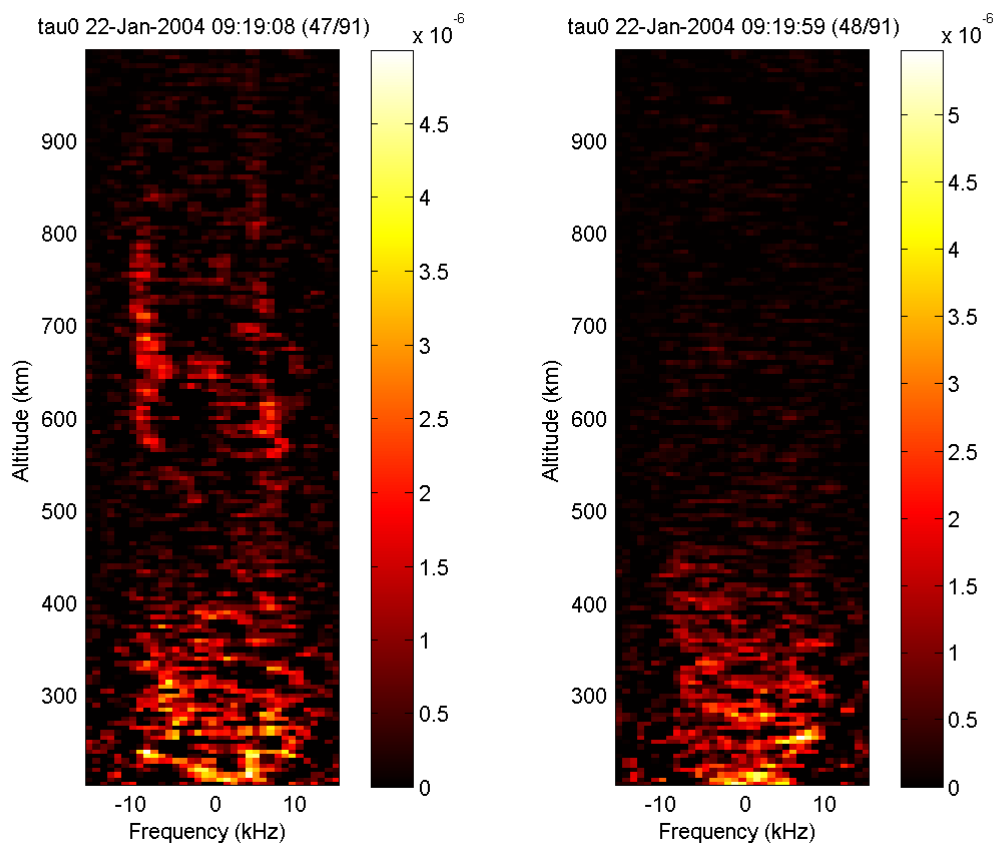


Figure 29: A couple of dumps that the histogram search method determined contained Neials. Only the left dump contains a Neial.

The difference between the first and second test may play an important role – the altitude range is significantly different between these two tests, where the first test spans from 200 to 600 *km*, and the second from 200 to 1000 *km*. It is conceivable that the histogram method operates best at lower altitudes, and fails at the upper altitudes. It is plausible that the noise in the very high altitudes

is too significant for this method to be applied in that region. Looking at Figure 29, this is a common result from the histogram method. While some dumps are relevant, there are many false positives reported.

In order to improve the accuracy of this method, a few parts of the algorithm were changed. Instead of clamping all powers in the spectra to a minimum of zero, all negative values were discarded instead, not counting in the rest of the procedures. The ratio x_n/\bar{x} was reduced to 5 and the parameters α and β were both set to 0.3. The effects were very significant.

Re-running the first test yielded five dumps. Of these five dumps, four were actual Neials and one was a false positive. No satellites were picked out. Compared to the previous test run, this is not much of an improvement; the method was still not able to pick out the last Neial, nor did it pick out the potential Neials.

The second test, however, is where the difference was clear. The method picked out 26 dumps, 19 of which were Neials, in addition to 2 potential (but faint) Neial. The method picked out a mere 5 satellites as well, a reduction in false positives of 93% and increase in Neials of 36%. While the method is still not picking out more than roughly two-thirds of the Neials, it may be used to quickly scan a large dataset to find interesting moments in time quickly. On its own, however, it will not be able to pick out a sufficiently large portion of the Neials, although it may be used to quickly find prominent Neials.

Spectral peak ratio

The examination of the spectral peak ratio is by far the slowest of the three methods, almost an order of magnitude slower than the histogram method. It is significantly more accurate on a wider range of datasets, however. This method performed reasonably well on both the tests, picking out the majority of Neials and avoided almost all satellites.

In the first test, this method selected 9 dumps out of 348 dumps to be a Neial. Of these nine dumps, 5 were actual Neials, none of them were satellites and 2 of them were false positives. The last 2 were potential Neials, although faint ones. This is an almost perfect result, where only one potential Neial was not picked up and only two dumps were false positives.

In the second test, this method performed a little worse, but it still had a strong performance. In this situation, it picked out a total of 47 dumps. Among these dumps, it found 26 actual Neials, 1 satellite and 16 false positives. 4 dumps were potential Neials, although very faint ones. While these results are worse than the first test, they are by no means useless. It should be noted that this method picked out very few satellites, reducing the amount of unwanted dumps.

The spectral peak ratio method can be used in all altitude ranges, as it only measures the ratio of the spectral peaks. A disadvantage of this method, however, is that if both the ion lines are enhanced at the same altitudes, this method will not be able to detect that Neial.

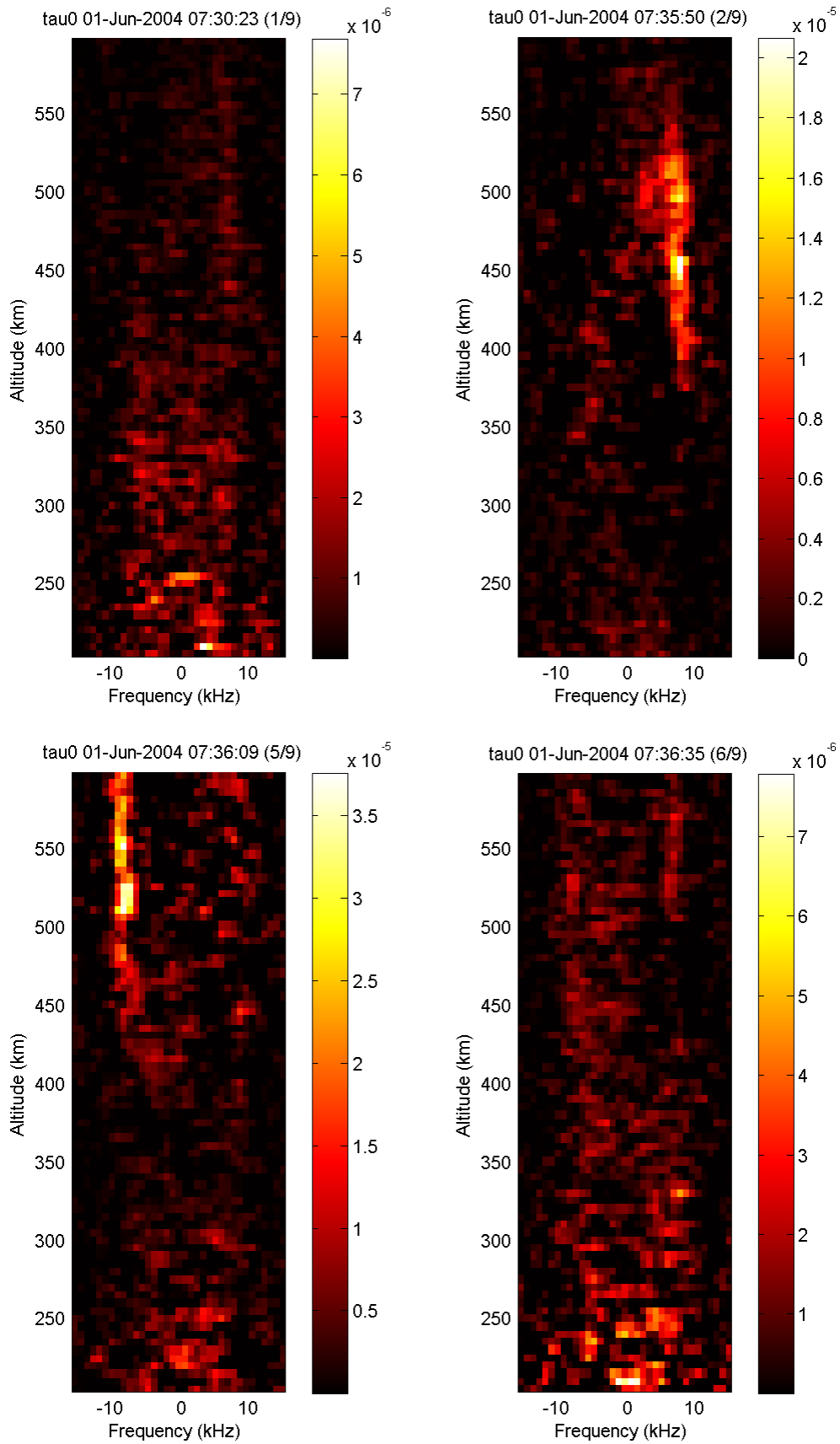


Figure 30: Some dumps picked out by the power profile method. The upper left and lower right panels are potential Neials, although they are rather faint. The other two panels are true positives that the method correctly reported.

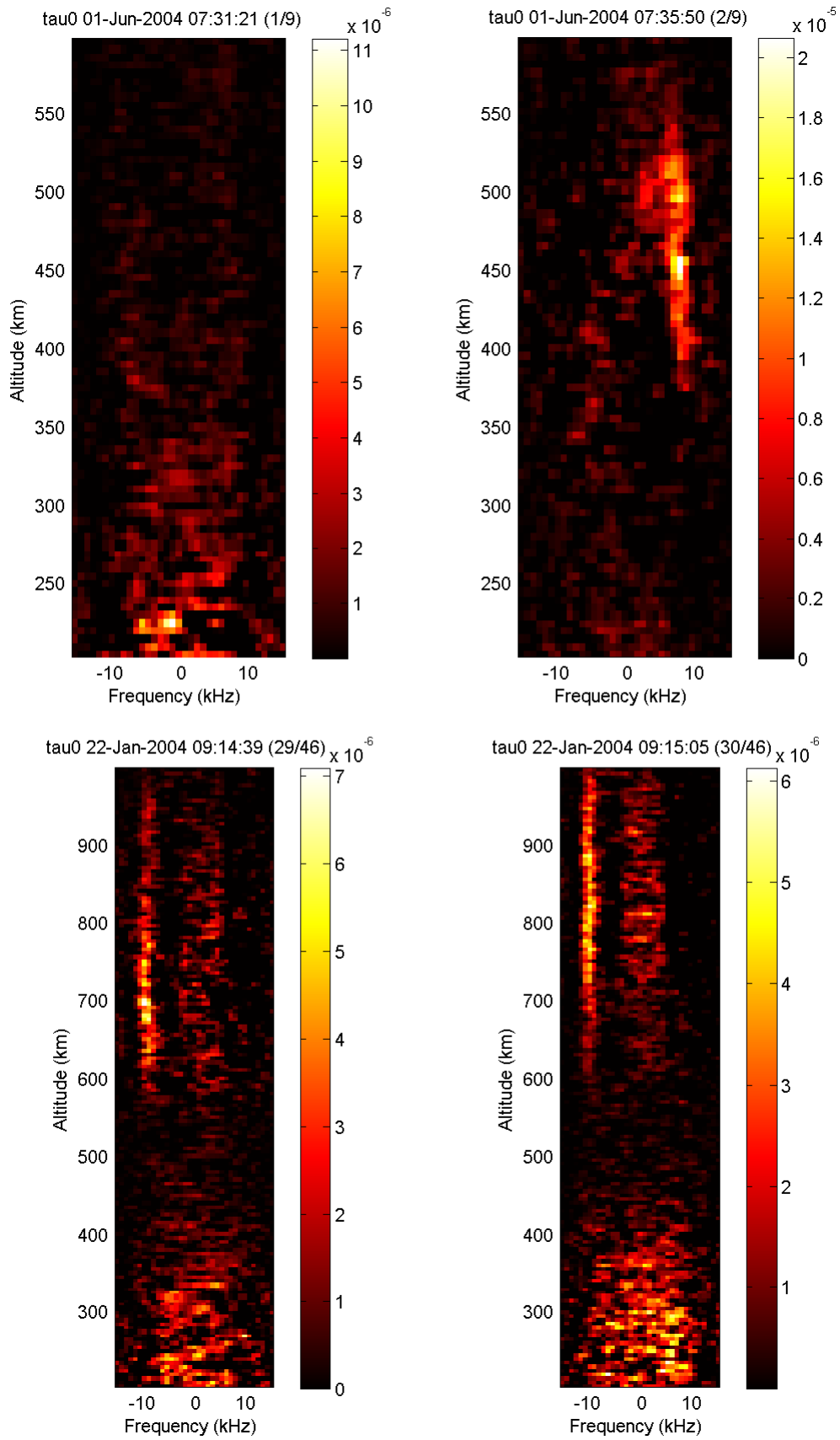


Figure 31: Some dumps picked out by the power profile method. The upper left panel is a false positive. The rest of the panels are true positives that the method correctly reported.

Power profile

Working with the power profile is significantly faster than examining the spectral peak ratio, although not as fast as examining at the histogram of the spectra. This method is more accurate than the histogram examination, although it is able to pick out approximately as many Neials as the spectral peak ratio method.

In the first test, a total of 9 out of 348 dumps were determined to be Neials by this method. 5 of these dumps were actual Neials, 2 were satellites and only 1 was a false positive. The last dump was a potential Neial. In this case, the method performed about equally well with the spectral peak method.

In the second test, the results differ slightly. In this case, a total of 46 dumps were chosen by the algorithm. Of these dumps, 27 were Neials, 11 were satellites and 6 were false positives. This is also roughly on par with the spectral peak ratio method, with the difference that this method picked out more satellites, and the spectral peak ratio method picked out more false positives.

One major weakness of this method is that it will falter at lower altitudes. The method strips away all data from altitudes lower than 400 *km* in order to avoid having to deal with the shape of the electron density function at the E- and F-layer. In addition, it will very often pick out satellites and other hard objects. Both these weaknesses might be eliminated, however, by taking into consideration the whole electron density profile, and by improving the satellite filtering algorithm.

Another inherent weakness of the method is that it might not be able to pick out faint Neials, as they are not strong enough to perturb the fitted curve enough. Attempting to force the method to select these dumps as well causes the method to select significantly more false positives. Contrasted to the spectral peak ratio method, it is clear that in this situation the latter method will be more efficient. On the other hand, in the situation where both ion-lines are simultaneously enhanced, the spectral peak ratio method will be unable to determine that there is a Neial there, whereas the power profile method will be able to “see” that Neial.

7.3 Discussion

At first, it would seem that the method of studying the histogram of the spectra is a too naïve method for detecting Neials. By introducing a very minor change, as mentioned in the previous section, the accuracy of the method is increased significantly. It is still not able to catch more than roughly two-thirds of all Neials, however, which is insufficient.

Turning the attention towards the spectral peak ratio method and the power profile method, it is apparent that both of them have certain regions they cannot be applied to. It should be noted that both methods can cover each other’s weaknesses, where the spectral peak ratio method can be applied to altitudes lower than 400 *km* and can relatively decently pick out faint Neials, and the power profile is capable of picking out Neials where both ion-lines are simultaneously enhanced.

This double-coverage suggests that it is feasible to combine both the methods, such that they work together on the same data to pick out as many Neials as possible. An obvious downside to this is that there will be more false positive reported, and more satellites polluting the end result. The processing speed will also be reduced significantly, although not by so much that the program is unable to run in real-time.

Combination of methods

If combining the spectral peak and power profile methods such that if either of them has determined that a Neial is present, then when running the same tests as before, they are able to pick out all five Neials in the first test, as well as the two potential Neials. They also picked out more false positives and satellites, however. In the second test, the picture is quite similar. In this case, both the methods were able to pick out almost all the Neials (29 out of 30 clear Neials) and many potential Neials as well. In total, 67 dumps were reported by this approach. The number of satellites and false positives was significant. Roughly half of the reported dumps were false positives or satellites.

Remembering back to the first method, the histogram examination, it is worth noting that the modified algorithm did not select many false positives, or satellites in either test. Thus it can be valuable to introduce this method to the combined algorithm as well. If the methods are combined such that if two of the three methods report a Neial on the same dumps, then that dump is considered to be containing a Neial.

In order to check how well these two ways to combine the methods operate, they were applied to the same two baseline tests. In the first test, the combination of the three methods was able to pick out all five Neials and one potential Neial, which is a very great result. No false positives, nor satellites, were reported in this case. In the second test, only 29 dumps were reported. Of these 29 dumps, 25 dumps were Neials and two were potential Neials, leaving only two dumps that were uninteresting. This approach was able to pick out roughly five out of every six Neial, which is decent.

The triple-combination was also tested on another data set, using the ESR 42m antenna, at June 29th, 2005, spanning from about 07:20:00 UT to 08:45:00 UT. In this new dataset, roughly eleven Neials could be counted by visual inspection, from roughly 4150 dumps. Out of these dumps, the combination between all three methods only reported a mere 29 dumps, eight of them which were actual Neials. This is the same number of Neials reported as the combination of the power profile and spectral peak ratio method, albeit with a significantly less number of irrelevant dumps. The spectral peak and power profile combination reported a total of 202 dumps, most of which were irrelevant dumps.

This suggests that combining the three methods, where only two of three has to report a Neial, is a far more accurate approach than relying on the combination of the spectral peak ratio and the power profile. While in most cases, the triple-combination reports fewer actual Neials and costs somewhat more processing time, it reports about an order of magnitude less irrelevant dumps than the duo-combination. When operating on datasets that span thousands if not tens of thousands of dumps, this makes a massive difference when going through the results, picking out the Neials among the false positives and satellites that passed the automated tests.

8 Conclusion and future work

This thesis shows that the process of automatically detecting Neials in EISCAT data is feasible and may be achieved by using several methods, which have different advantages and disadvantages. By utilizing these methods in various combinations, it is possible for a program to detect more Neials at the cost of finding more false positives, or reduce the number of false positive at the cost of actual Neials.

Improvements of the individual methods are still possible. By taking into account the full electron density distribution function, the power profile method may be significantly improved, reducing the number of false positives it selects. Improvements in the modeling of the spectral peaks and their magnitudes can improve the accuracy of the spectral peak method. By improving the satellite detection algorithm, it may be possible to reduce the number of false positives due to satellites significantly.

With a program that is able to detect Neials, the task of locating the Neials in the EISCAT data will be an easier task to perform, and will require significantly less time. By allowing Neials to be more accessible, studies on this phenomenon may be performed more easily, allowing the understanding of the ionosphere, the geophysical processes that take place, as well as the physics, to improve.

Code

Main program

In order to utilize the program itself, once all the other functions have been obtained, the program may be utilized by running this example code:

```
directory = 'C:\directory\containing\data';
files = findNeials(directory, 2, 0);
displayNeials(files, directory, 'neial');
```

findNeials.m

This function is the main entry of the program, and is responsible of locating Neials. It will iterate through all the MatLab-files it can find in the provided directory, and see which one of them that contains a Neial.

```
function [ r_files ] = findNeials( p_path, p_sensitivity, p_displayInfo )
%FINDNEIALS Returns files that contains a Neial under the specified path
% Inputs:
%   p_path: Path to the directory containing the data dumps
%   p_sensitivity: How picky the program is, the higher values the
%                 less false positives are given, but fewer Neials
%                 will be found.
%                 1: Somewhat prone to noise, finds almost all Neials
%                 2: Picks out less noise, but also fewer Neials
%                 3: Finds almost only Neials, but less of them
%   p_displayInfo: How to display the work in progress of the program.
%                 -1: Displays no information
%                 0: Displays which files are currently being
%                 processed
%                 1: Displays the spectra that are being processed
%                 2: Displays and saves the spectra that are being
%                 processed
% Returns:
%   r_files: A list of files the program believes to contain Neials
% Example: findNeials('C:\My folder\data', 2, 0);
% Will traverse the entire directory that has been provided, looking for
% files that contains Neials. These files will then be returned as a
% list.

index = 1;
r_files = {};

% Prepare displaying of info
if (p_displayInfo == 1 || p_displayInfo == 2)
    h = figure;
end

% Start looking for Neials
q = dir([p_path, '\*.mat']);
for i1 = 1 : length(q)
    load([p_path, '\', q(i1).name]);
    if p_displayInfo >= 0
        disp(['[', datestr(now), '] Examining ', datestr(r_time(1,:)), ...
            ' (', int2str(i1), ' / ', int2str(length(q)), ')...']);
    end
end
```

```

end

foundNeial = 0;

% Perform the Neial search algorithms
[rHistogram] = searchSpectrumHistogram(r_spec);
[rPowerProfile] = searchSpectrumPowerProfile(r_spec, r_freq, r_range);
[rPeakRatio] = searchSpectrumRatio(r_spec, r_freq, r_range);
if (rHistogram + rPowerProfile + rPeakRatio >= p_sensitivity)
    foundNeial = 1;
end

% If a Neial was found, store it for later use
if (foundNeial == 1)
    r_files{index} = q(i1).name;
    index = index + 1;
end

% If enabled by the user, display information about what is going on
if (p_displayInfo == 1 || p_displayInfo == 2)
    if (mod(i1 + 1, 2) == 0)
        p_freq = r_freq;
        p_spec = r_spec;
        p_range = r_range;
        p_time = r_time;
    end
    if (mod(i1 + 1, 2) == 1 || i1 == length(q))
        clf(h);
        subplot(1, 2, 1);
        pcolor(p_freq'/1e3, p_range, max(0, p_spec')), ...
            shading flat, colormap(hot(256)), ...
            colorbar('location','EastOutside');
        title([name_expr, ' ', datestr(p_time(1,:)), ' UT']);
        xlabel('Frequency (kHz)');
        ylabel('Altitude (km)');
        if (i1 ~= length(q))
            subplot(1, 2, 2);
            pcolor(r_freq'/1e3, r_range, max(0, r_spec')), ...
                shading flat, colormap(hot(256)), ...
                colorbar('location','EastOutside');
            title([name_expr, ' ', datestr(r_time(1,:)), ' UT']);
            xlabel('Frequency (kHz)');
            ylabel('Altitude (km)');
        end
        drawnow;

        if (p_displayInfo == 2)
            saveas(h, [p_path, '\', name_expr, ' ', ...
                strrep(datestr(p_time(1,:)), ':', '_)], 'png');
        end
    end
end
end
end
end

```

displayNeials.m

The display function is added for the convenience of the user. It will automatically display the spectra to the user and store them under the user-specified name, in the provided folder.

```
function [ ] = displayNeials( p_files, p_path, p_name )
%DISPLAYNEIALS Displays the Neials there were found using the findNeials
%function.
% Inputs:
%   p_files: A list of files that are going to be displayed
%   p_path: The path to the folder containing all the files
%   p_name: The prefix for the name the plots should be saved under
%
% Example: displayNeials(findNeials(...), 'C:\My folder\data', 'neial');

h = figure;
for il = 1 : 2 : length(p_files)
    clf(h);
    subplot(1, 2, 1);
    load([p_path, '\', p_files{il}]);
    pcolor(r_freq'/1e3, r_range, max(0, r_spec')), shading flat, ...
        colormap(hot(256)), colorbar('location','EastOutside');
    title([name_expr, ' ', datestr(r_time(1,:)), ' UT']);
    xlabel('Frequency (kHz)');
    ylabel('Altitude (km)');

    if (il ~= length(p_files))
        subplot(1, 2, 2);
        load([p_path, '\', p_files{il + 1}]);
        pcolor(r_freq'/1e3, r_range, max(0, r_spec')), shading flat, ...
            colormap(hot(256)), colorbar('location','EastOutside');
        title([name_expr, ' ', datestr(r_time(1,:)), ' UT']);
        xlabel('Frequency (kHz)');
        ylabel('Altitude (km)');
    end

    drawnow;
    saveas(h, [p_path, '\', p_name, '_', ...
        strrep(datestr(r_time(1,:)), ':', '_')], 'png');
end

end
```

searchSpectrumHistogram.m

The histogram algorithm is implemented according to the code displayed here:

```
function [r_result] = searchSpectrumHistogram(p_spectrum)
% Returns whether the given spectrum contains an anomaly or not
% Returns:
%   r_result: Boolean, is true if a Neial was potentially found
%
% Will traverse the entire spectrum, looking for Neials. If a Neial
% was located, the algorithm will terminate early and return true.
% This algorithm will perform a smoothing of the spectrum internally,
% then iterate from the bottom and up until it determines that it has
% found a Neial or until it reaches the top of the spectrum.
```



```

% Smooth out the spectrum slightly, to reduce noise
p_spectrum = filter2(fspecial('average', 3), p_spectrum);

r_result = false;

gatesInRow = 0;
lastGate = -1;
for y = 1 : size(p_spectrum, 2)
    % Compute the average of the spectrum after removing the top/bottom
    % values; will attempt to grab only the average of the actual spectrum,
    % and not the background noise values

    values = p_spectrum(:, y);
    values = sort(values(values > 0));
    lower_bound = max(1, ceil(0.3 * length(values)));
    upper_bound = min(length(values), floor(0.7 * length(values)));
    gate_mean = mean(values(lower_bound : upper_bound));

    for x = 1 : size(p_spectrum, 1)
        % Detect significant variation from the average
        d = p_spectrum(x, y) / gate_mean;
        if (d > 5)
            % Only care about gates that are in close proximity; distant
            % gates may exist, but are not relevant
            if (abs(lastGate - y) < 4 || lastGate == -1)
                gatesInRow = gatesInRow + 1;
            else
                gatesInRow = 0;
            end
            lastGate = y;

            % Once enough gates are thought of to contain a Neial, return
            if (gatesInRow > 5)
                r_result = true;
                return;
            end
            break;
        end
    end
end
end
end

```

searchSpectrumPowerProfile.m

The power profile algorithm is implemented according to the code displayed here:

```

function [ r_result ] = searchSpectrumPowerProfile(p_spectrum, p_frequency,
p_range)
% Returns whether the given spectrum contains an anomaly or not
% Returns:
%     r_result: Boolean, is true if a Neial was potentially found
%
% Will convert the spectrum into a power profile, then attempt to see how
% well an exponential curve can be fitted to it. If the curve is
% ill-fitting, then the algorithm has potentially found a Neial.

% Integrate the spectra over frequency

```

```

profile = zeros(1, size(p_spectrum, 2));
for i1 = 1 : size(p_spectrum, 2)
    profile(i1) = trapz(p_frequency(:, i1), max(0, p_spectrum(:, i1)));
end

% Grab the power profile and trim away everything below 300km
index = 1;
for i1 = 1 : size(p_range, 1)
    if (p_range(i1) < 400)
        index = index + 1;
    else
        break;
    end
end
p_range = p_range(index : end);
profile = profile(index : end);

% Filter away satellites
width = 10;
tmpProfile = profile;
for i1 = 1 : length(profile)
    if (i1 < width + 1)
        value = profile(i1 + width);
    elseif (i1 > length(profile) - width)
        value = profile(i1 - width);
    else
        value = min(profile(i1 - width), profile(i1 + width));
    end
    ratio = profile(i1) / value;
    if (ratio > 7.5)
        tmpProfile(i1) = value;
    else
        tmpProfile(i1) = profile(i1);
    end
end

% Smooth data and calculate the exponential curve
profile = smooth(tmpProfile, 3);
f = fit(p_range, profile, 'exp1');

% Analyze the exponential curve
correlation = sqrt(sum((f.a * exp(f.b * p_range) - profile).^2) /
    (length(profile) - 1));
if (f.b > 0 || correlation > 2 * 10^-3)
    r_result = 1;
else
    r_result = 0;
end

end

```

searchSpectrumRatio.m

The spectral peak ratio algorithm is implemented according to the code displayed here:

```

function [r_result] = searchSpectrumRatio(p_spectrum, p_frequency, p_range)
% Returns whether the given vector contains an anomaly or not
% Returns:
%     r_result: Boolean, is true if a Neial was potentially found

```

```

%
% Will traverse the entire spectrum, looking for Neials. If a Neial
% was located, the algorithm will terminate early and return true.

r_result = false;
p_spectrum = max(0, filter2(fspecial('average', 3), p_spectrum));

% Tracking the smallest nonzero peak
largest = 0;
gates = {};

% Iterate over all gates...
for y = 1 : size(p_spectrum, 2)
    spectrumGate = p_spectrum(:, y);
    frequencyGate = p_frequency(:, y);
    [spec, freq] = findSpectralPeaks(spectrumGate, frequencyGate);

    % Find the largest value
    lastLargest = largest;
    largest = max(spec);

    % Calculate the difference between the peaks and the frequencies, the
    % frequency and the height
    a = abs(spec(1) - spec(2)) / max(largest, lastLargest);
    if (spec(1) > spec(2))
        frequency = freq(1);
    else
        frequency = freq(2);
    end
    height = p_range(y);

    % Skip all locations where a < 0.6, and where W_l and W_r aren't within
    % 5kHz of consecutive gates
    if (a > 0.6)
        gates{end + 1} = struct('height', height, 'frequency', frequency);

        % Check for some gates within 25km and 5kHz of the current gate
        count = 0;
        for i1 = 1 : length(gates) - 1
            gate = gates{i1};
            if (abs(gate.height - height) < 25 && ...
                abs(gate.frequency - frequency) < 5e3)
                count = count + 1;
                if (count >= 5)
                    r_result = true;
                    return;
                end
            end
        end
    end
end
end
end
end
end
end

```

findSpectralPeaks.m

In order to calculate the ratio of the spectral peaks for any given spectra, a method of obtain them was constructed. The algorithm to do so was implemented according to

```

function [r_spec, r_freq] = findSpectralPeaks(p_spectrum, p_frequency)
%FINDSPECTRALPEAKS Will return the locations (x-values) of the peaks
% The function will traverse the vector p_spectrum, looking for values
% that are local maxima. This will be heavily biased towards what it
% expects a usual spectrum to look like, thus it will attempt to
% model a proper spectrum structure regardless of noise level.

% Modulate the spectrum by removing peaks in the middle and edges

indices = find(abs(p_frequency) < 5e3);
p_spectrum(indices) = p_spectrum(indices) .* (abs(p_frequency(indices)) /
5.5e3).^2;
indices = find(abs(p_frequency) > 10e3);
modulatedSpectrum = p_spectrum;
modulatedSpectrum(indices) = p_spectrum(indices) .* max(0,
((abs(p_frequency(indices)) - 10e3) / 15e3));

% Find all the peaks in the modulated spectrum
[~, l] = findpeaks(modulatedSpectrum);

indices = l(p_frequency(l) < 0);
spec{1} = p_spectrum(indices);
freq{1} = p_frequency(indices);
indices = l(p_frequency(l) > 0);
spec{2} = p_spectrum(indices);
freq{2} = p_frequency(indices);

% The expected location of the spectral peaks
peaks(1) = -8e3;
peaks(2) = 8e3;

r_spec = [0, 0];
r_freq = [0, 0];

% Calculate the contributon from each peak
for side = 1 : 2
    weight = 0;
    largestValue = max(spec{side});

    for i1 = 1 : length(freq{side})
        factor = max(0, 1 - abs(peaks(side) - freq{side}(i1)) / 10e3);
        factor = factor * abs(spec{side}(i1) / largestValue)^2;
        weight = weight + factor;

        r_spec(side) = r_spec(side) + factor * spec{side}(i1);
        r_freq(side) = r_freq(side) + factor * freq{side}(i1);
    end
    if weight == 0
        r_spec(side) = 0;
        r_freq(side) = peaks(side);
    else
        r_spec(side) = r_spec(side) / weight;
        r_freq(side) = r_freq(side) / weight;
    end
end
end
end

```

Final notes

The code presented in this thesis is released as free software under the GNU General Public License, published by the Free Software Foundation. The code may be redistributed and/or modified, under version 3 of the License, or any later version of the reader's choice.

Acknowledgement

First and foremost, a big thanks to my supervisor, Prof. Unni Pia Løvhaug for all the support, continuous feedback, praise and criticism alike, and the many discussions we had. You have shown me the importance of an open and inquiring mind, and your enthusiasm has definitely rubbed over onto me.

Thanks to Prof. Björn Gustavsson, without your help on the technical parts of Guisdap, this project would likely never have gotten anywhere.

While somewhat cliché, I would also like to thank my family and friends as well, for their support and their help, as well as the much needed distractions they provided.

Bibliography

Beynon, W. J. G., and P. J. S. Williams, Incoherent scatter of radio waves from the ionosphere, *Reports on Progress in Physics*, 41, 909-956, doi:10.1088/0034-4885/41/6/003, 1978.

Bjørnå, N.: AGF-304 Radar diagnostics of space plasma, Lecture Notes Fys-3002, UiT, The Arctic University of Norway, 2005.

Brekke, A.: *Physics of the Upper Polar Atmosphere*, second edition, 2013, ISBN 978-3-642-27400-8.

Buchert, S. C., van Eyken, A. P., Ogawa, T., and Watanabe, S.: Naturally enhanced ion-acoustic lines seen with the EISCAT Svalbard Radar, *Adv. Space Res.*, 23, 1699-1704, 1999

Chen, F., F.: *Introduction to Plasma Physics and Controlled Fusion, Volume 1*, second edition, 1984, ISBN: 0-306-41332-9.

Collis, P. N., Häggström, I., Kaila, K. and Rietveld, M. T.: EISCAT radar observations of enhanced incoherent scatter spectra; their relation to red aura and field-aligned currents, *Geophys. Res. Lett.*, 18, 1031-1034, 1991.

EISCAT Scientific Association (2016), <https://www.eiscat.se>.

Farley, D. and T. Hagfors: Incoherent scatter theory, Lecture Notes Fys-3002, UiT, The Arctic University of Norway.

Forme, F. R. E.: A new interpretation on the origin of enhanced ion acoustic fluctuations in the upper ionosphere, *Geophys. Res. Lett.*, 20, 2347–2350, 1993

Forme, F. R. E.: Parametric decay of beam-driven Langmuir wave and enhanced ion-acoustic fluctuations in the ionosphere: a weak turbulence approach, *Ann. Geophys.*, 17, 1172-1181, doi:10.1007/s00585-999-1172-4, 1999.

Forme, F. R. E. and Fontaine, D.: Enhanced ion acoustic fluctuations and ion outflows, *Ann. Geophys.*, 17, 182-189, 1999.

Foster, J. C., del Pozo, C., Groves, K., and St. Maurice, J.-P.: Radar observations of the onset of current driven instabilities in the topside ionosphere, *Geophys. Res. Lett.*, 15, 160-163, 1988.

Grydeland, T., La Hoz, C., Hagfors, T., Blixt, E. M., Saito, S., Strømme, A., and Brekke, A.: Interferometric observations of filamentary structures associated with plasma instability in the auroral ionosphere, *Geophys. Res. Lett.*, 30, 1338, doi:10.1029/2002GL016362, 2003

Lunde, J., Gustavsson, B., Løvhaug, U. P., Lorentzen, D. A., and Ogawa, Y.: Particle precipitations during NEIAL events: simultaneous ground based observations at Svalbard, *Ann. Geophys.*, 25, 1323-1336, doi:10.5194/angeo-25-1323-2007, 2007.

Neubert, T. and Christiansen, F.: Small-scale field-aligned currents at the top-side of the ionosphere, *Geophys. Res. Lett.*, 30, 2010, doi:10.1029/2003GL017808, 2003

Nygrén, T.: *Introduction to Incoherent Scatter Measurements*, Invers., 1996

Ogawa, Y., Buchert, S. C., Fujii, R., Nozawa, S., and Forme, F.: Naturally enhanced ion-acoustic lines at high altitudes, *Ann. Geophys.*, 24, 3351-3364, doi:10.5194/angeo-24-3351-2006, 2006.

Ogawa, Y., S. C. Buchert, I. Häggström, M. T. Rietveld, R. Fujii, S. Nozawa, and H. Miyaoka: On the statistical relation between ion upflow and naturally enhanced ion-acoustic lines observed with the EISCAT Svalbard radar, *J. Geophys. Res.*, 116, A03313, doi:10.1029/2010JA015827, 2011.

Rietveld, M. T., Collis, P. N., and St.-Maurice, J.-P.: Naturally Enhanced Ion Acoustic Waves in the Auroral Ionosphere Observed With the EISCAT 933-MHz Radar, *J. Geophys. Res.*, 96, 19291-19305, 1991.

Rosenbluth, M. N., and N. Rostoker: Scattering of electromagnetic waves by nonequilibrium plasma, *Physics of Fluids*, 5(7), 776–788, doi:doi:10.1063/1.172446, 1962

Strømme, A., V. Belyey, T. Grydeland, C. La Hoz, U. P. Løvhaug, and B. Isham: Evidence of naturally occurring wave-wave interactions in the polar ionosphere and its relation to naturally enhanced ion acoustic lines, *Geophys. Res. Lett.*, 32, L05103, doi:10.1029/2004GL020239, 2005.

Trulsen, J. and N. Bjørnå: The origin and properties of thermal fluctuations in a plasma, In *Radar Probing of the Auroral Plasma*, ed. A. Brekke, 1975

Wahlund, J.-E., H. J. Opgenoorth, I. Häggström, K. J. Winser, and G. O. L. Jones : EISCAT Observations of Topside Ionospheric Ion Outflows During Auroral Activity: Revisited, *J. Geophys. Res.*, 97(A3), 3019–3037, doi:10.1029/91JA02438, 1992a.

Wahlund, J.-E., Forme, F. R. E., Opgenoorth, H. J., Persson, M. A. L., Mishin, E. V., and Volokitin, A. S.: Scattering of electromagnetic waves from a plasma: enhanced ion acoustic fluctuations due to ion-ion two-stream instabilities, *Geophys. Res. Lett.*, 19, 1919-1922, 1992b.

Nomenclature

e	Electron charge
ε_0	Permittivity of free space
κ	Boltzmann constant
m_e	Mass of electrons
m_i	Mass of ions
n_0	Mean number density
n_e	Electron number density
T_e	Temperature of electrons
T_i	Temperature of ions
NaN	Not a number
Neial	Naturally enhanced ion-acoustic line
VHF	Very high frequency
UHF	Ultra high frequency

